

15. PIOCENE STABLE ISOTOPE STRATIGRAPHY OF SITE 846¹

N.J. Shackleton,² M.A. Hall,² and D. Pate²

ABSTRACT

Oxygen and carbon isotope ratios were measured in benthic foraminifers from the entire Pliocene and latest Miocene sections of Site 846, a 180-m section, at a sampling interval of 10 cm. This provides a temporal resolution of about 2500 yr. The documented continuity of the record is excellent. Using the time scale that was developed on the basis of orbital tuning of GRAPE density records, we observed a fairly constant phase relationship between $\delta^{18}\text{O}$ and variations in the obliquity of Earth's rotational axis. A new numbering scheme for Pliocene isotope stages is proposed.

This high-resolution $\delta^{18}\text{O}$ record clarifies several interesting aspects of late Neogene climatic evolution, including a "glacial" event that may have caused the final Messinian desiccation of the Mediterranean Sea; one or more "interglacial" events that might have caused refilling of the Mediterranean; a well-resolved couplet of glacial events at about the age of the Sidujfall Subchron; interglacial extremes in the early part of the Gauss that could have resulted from either significant deglaciation on Antarctica or from warming of deep water; and a gradual ramp of increasingly extreme "glacial" events, starting at about the Kaena Subchron and culminating with $\delta^{18}\text{O}$ stage 100 in the earliest Matuyama.

INTRODUCTION

In the Pacific Ocean, the best high-resolution $\delta^{18}\text{O}$ record available at the time of Ocean Drilling Program (ODP) Leg 138 was Site 677 (Becker, Sakai, et al., 1988). Double APC-coring at Site 677 was limited to the last 2.5 m.y.; over this interval, a high-resolution $\delta^{18}\text{O}$ record was obtained (Shackleton and Hall, 1989; Appendix) that permitted an astronomical calibration of the $\delta^{18}\text{O}$ record and, hence, of the geological time scale since 2.5 Ma (Shackleton et al., 1990). One objective of Leg 138 was to extend this astronomical age calibration of the $\delta^{18}\text{O}$ record as far as possible into the Neogene. Of the 11 sites drilled during Leg 138, Site 846 was selected as offering an excellent opportunity for obtaining an extended high-resolution benthic $\delta^{18}\text{O}$ record. The Pleistocene section was analyzed in Oregon by Mix (see Le et al., this volume); in this chapter, we discuss the Pliocene and latest Miocene sections. Shipboard analysis indicated that the sedimentation rate was about 40 m/m.y., so that the site is capable of providing good resolution of variability in the range of Earth's orbital variations (periods 20 to 100 k.y.). Site 846 is located to the south of the Galapagos Islands, at 3°5.80'S, 90°49.07'W in a water depth of 3296 m.

METHODS

The continuity of the sedimentary sequence at Site 846 was established aboard the *JOIDES Resolution* by constructing composite sections on the basis of gamma-ray attenuation porosity evaluator (GRAPE) density, color, and magnetic-susceptibility records (Hagelberg et al., 1992) in the overlapping holes that were cored. On the basis of the composite depth sections developed by Hagelberg et al. (1992), the site was sampled at 10-cm intervals to provide a continuous record, using Hole 846D where possible, and incorporating sections from Holes 846B and 846C to cover stratigraphic gaps between successive cores in Hole 846D. This strategy enabled us to obtain a complete section without significant stratigraphic duplication (which wastes both valuable core material and laboratory time). Shipboard examination of core-catcher material indicated that 10-cm³ samples generally should provide sufficient benthic foraminifers for isotopic analysis, and this proved to be the case.

In Cambridge, samples were washed on a 150- μm sieve using distilled water, oven-dried on the sieves at 60°C, and then weighed. The fine fraction was collected and settled overnight, after which the water was siphoned off to just above the sediment surface. The residue was dried and weighed so that the percentage over 150 μm could be determined. Because the coarse fraction contains some pyrite and radiolarian skeletons, the weight over 150 μm only provides a rough estimate of weight of foraminiferal material over a cutoff of this size; the data are given in Table 1. (Note: Tables 1, 3, 5, 6, 7, and 9 can be found on the CD ROM at the back of the volume and are not printed here.)

Specimens for isotopic analysis were selected under a low-power ($\times 25$) binocular microscope. Species were picked with a first priority being the generation of a reliable $\delta^{18}\text{O}$ record; to maintain consistency with other $\delta^{18}\text{O}$ records from the eastern Pacific Ocean, *Uvigerina* spp. were selected where they were sufficiently abundant. To maximize the value of the $\delta^{13}\text{C}$ record from *Uvigerina*, we tried to select only the larger specimens of *U. senticosa* that are characteristic of the high-productivity eastern Pacific Ocean, where this was possible. Shackleton and Pisias (1985) used this species for developing the $\delta^{13}\text{C}$ record of Core V19-30 and Mix et al. (1991) showed that this species reliably records $\delta^{13}\text{C}$ in the eastern equatorial Pacific. At intervals throughout the sequence, specimens of *Cibicides wuellerstorfi* and/or of *C. kullenbergi* were chosen in parallel to *Uvigerina* spp. to check on the consistency of the interspecific isotopic differences. Several studies have verified the $\delta^{18}\text{O}$ and $\delta^{13}\text{C}$ differences between *Uvigerina* spp. and *C. wuellerstorfi* obtained by Shackleton and Opdyke (1973). Farrell (1991) made a careful evaluation that shows that for isotopic purposes, *C. wuellerstorfi* and *C. kullenbergi* are interchangeable. Where it was not possible to select the above species, *Oridorsalis umbonifera*, *Globobulimina pacifica*, *Sphaeroidina bulloides*, *Globocassidulina subglobosa*, or mixtures of the above were selected, while accepting that the $\delta^{13}\text{C}$ data might be valueless.

Wherever possible, between 6 and 12 specimens were selected for each analysis. However, for many of the analyses of *G. pacifica*, as few as three specimens were used. Specimens showing anomalous preservation were avoided on the basis that they may have been reworked, as were abnormally large specimens. The selected specimens were lightly crushed and soaked in hydrogen peroxide (10 vols) to remove any possible organic contaminants. Analytical grade acetone was then added, and the samples cleaned ultrasonically, after which the excess liquid was siphoned off. The samples were dried in an oven at 60°C before being transferred to small glass boats ready for analysis. Carbon diox-

¹ Pisias, N.G., Mayer, L.A., Janecek, T.R., Palmer-Julson, A., and van Andel, T.H. (Eds.), 1995. *Proc. ODP, Sci. Results*, 138: College Station, TX (Ocean Drilling Program).

² University of Cambridge, Godwin Laboratory, Free School Lane, Cambridge CB2 3RS, United Kingdom.

Table 1. Percentage of coarse fraction data for Site 846.

Core, section, interval (cm)	Depth (mbsf)	Depth (mcd)	Depth (rmcd)	150 (g)	150 (g)	cf (%)
138-846B-						
7H-1, 75-77	55.25	63.55	63.43	0.16	4.93	3.14
7H-1, 85-87	55.35	63.65	63.53	0.13	4.99	2.54
7H-1, 95-97	55.45	63.75	63.63	0.16	5.91	2.64
7H-1, 105-107	55.55	63.85	63.72	0.10	5.15	1.90
7H-1, 115-117	55.65	63.95	63.82	0.24	6.48	3.57
7H-1, 127-129	55.77	64.07	63.94	0.33	6.58	4.78
7H-1, 135-137	55.85	64.15	64.03	0.35	5.89	5.61
7H-1, 145-147	55.95	64.25	64.15	0.22	4.83	4.36
7H-2, 5-7	56.05	64.35	64.28	0.13	4.64	2.73
7H-2, 13-15	56.13	64.43	64.39	0.19	3.46	5.21
7H-2, 25-27	56.25	64.55	64.54	0.07	4.19	1.64
7H-2, 35-37	56.35	64.65	64.65	0.13	4.15	3.04
7H-2, 45-47	56.45	64.75	64.76	0.09	4.12	2.14
7H-2, 55-57	56.55	64.85	64.86	0.04	4.43	0.89
7H-2, 65-67	56.65	64.95	64.96	0.06	4.63	1.28
7H-2, 77-79	56.77	65.07	65.08	0.06	4.54	1.30
7H-2, 86-88	56.86	65.16	65.16	0.07	4.94	1.40
7H-2, 95-97	56.95	65.25	65.25	0.07	4.48	1.54
7H-2, 106-108	57.06	65.36	65.35	0.05	4.53	1.09
7H-2, 115-117	57.15	65.45	65.44	0.07	4.89	1.41
7H-2, 125-127	57.25	65.55	65.54	0.06	4.54	1.30
7H-2, 135-137	57.35	65.65	65.65	0.10	4.91	2.00
7H-2, 145-147	57.45	65.75	65.75	0.14	5.00	2.72
7H-3, 5-7	57.55	65.85	65.85	0.09	3.66	2.40
7H-3, 15-17	57.65	65.95	65.96	0.09	4.35	2.03
7H-3, 25-27	57.75	66.05	66.06	0.09	3.91	2.25
7H-3, 35-37	57.85	66.15	66.16	0.08	4.48	1.75
7H-3, 45-47	57.95	66.25	66.26	0.05	3.78	1.31
7H-3, 55-57	58.05	66.35	66.36	0.06	4.72	1.26
7H-3, 65-67	58.15	66.45	66.45	0.07	4.03	1.71
7H-3, 77-79	58.27	66.57	66.56	0.08	4.08	1.92
7H-3, 86-88	58.36	66.66	66.65	0.06	4.04	1.46
7H-3, 95-97	58.45	66.75	66.74	0.07	3.95	1.74
7H-3, 106-108	58.56	66.86	66.85	0.22	4.51	4.65
7H-3, 115-117	58.65	66.95	66.94	0.09	4.52	1.95
7H-3, 124-126	58.74	67.04	67.03	0.07	4.27	1.61
7H-3, 135-137	58.85	67.15	67.14	0.05	4.11	1.20
7H-3, 145-147	58.95	67.25	67.24	0.06	4.56	1.30
7H-4, 5-7	59.05	67.35	67.34	0.05	3.77	1.31
7H-4, 12-14	59.12	67.42	67.41	0.03	4.24	0.70
7H-4, 24-26	59.24	67.54	67.52	0.05	3.38	1.46
8H-1, 25-27	64.25	74.45	74.30	0.07	5.01	1.38
8H-1, 34-36	64.34	74.54	74.36	0.09	5.21	1.70
8H-1, 45-47	64.45	74.65	74.45	0.09	5.96	1.49
8H-1, 55-57	64.55	74.75	74.62	0.11	6.11	1.77
8H-1, 65-67	64.65	74.85	74.81	0.11	5.91	1.83
8H-1, 75-77	64.75	74.95	75.01	0.12	5.68	2.07
8H-1, 86-88	64.86	75.06	75.25	0.25	3.99	5.90
8H-1, 95-97	64.95	75.15	75.34	0.40	4.31	8.49
8H-1, 105-107	65.05	75.25	75.39	0.36	4.12	8.04
8H-1, 115-117	65.15	75.35	75.44	0.20	3.78	5.03
8H-1, 125-127	65.25	75.45	75.47	0.15	4.65	3.13
8H-1, 135-137	65.35	75.55	75.52	0.26	4.69	5.25
8H-1, 145-147	65.45	75.65	75.56	0.29	3.11	8.53
8H-2, 5-7	65.55	75.75	75.62	0.09	3.95	2.23
8H-2, 15-17	65.65	75.85	75.70	0.08	4.91	1.60
8H-2, 25-27	65.75	75.95	75.82	0.10	5.43	1.81
8H-2, 35-37	65.85	76.05	75.98	0.08	4.57	1.72
8H-2, 46-48	65.96	76.16	76.16	0.10	4.45	2.20
8H-2, 55-57	66.05	76.25	76.26	0.07	4.06	1.69
8H-2, 65-67	66.15	76.35	76.36	0.07	4.47	1.54
8H-2, 78-80	66.28	76.48	76.47	0.08	4.23	1.86
8H-2, 85-87	66.35	76.55	76.54	0.13	4.73	2.67
8H-2, 94-96	66.44	76.64	76.63	0.10	4.25	2.30
8H-2, 105-107	66.55	76.75	76.76	0.11	4.00	2.68
8H-2, 115-117	66.65	76.85	76.85	0.08	4.17	1.88
8H-2, 125-127	66.75	76.95	76.95	0.08	3.18	2.45
8H-2, 135-137	66.85	77.05	77.06	0.12	4.11	2.84
8H-2, 145-147	66.95	77.15	77.17	0.09	4.88	1.81
8H-3, 5-7	67.05	77.25	76.76	0.07	3.99	1.72
8H-3, 15-17	67.15	77.35	76.85	0.04	3.04	1.30
8H-3, 25-27	67.25	77.45	76.95	0.07	3.83	1.79
8H-3, 35-37	67.35	77.55	77.06	0.05	3.32	1.48
8H-3, 45-47	67.45	77.65	77.17	0.04	3.80	1.04
8H-3, 55-57	67.55	77.75	77.26	0.02	3.81	0.52
8H-3, 65-67	67.65	77.85	77.35	0.05	3.87	1.28
8H-3, 77-79	67.77	77.97	77.46	0.05	4.32	1.14
8H-3, 86-88	67.86	78.06	77.56	0.06	4.24	1.40
8H-3, 95-97	67.95	78.15	77.65	0.08	4.27	1.84
8H-3, 106-108	68.06	78.26	77.76	0.05	4.48	1.10
8H-3, 116-118	68.16	78.36	77.86	0.05	4.16	1.19
8H-3, 125-127	68.25	78.45	77.95	0.20	4.24	4.50

Only the first page of this table is reproduced here. The entire table appears on the CD-ROM (backpocket).

ide for isotopic analysis was released using orthophosphoric acid at 90°C in a VG Isocarb common acid bath system and analyzed on line in a VG Isotech PRISM triple collector mass spectrometer. Each run comprised five standard marble aliquots, a blank (empty container), 20 foraminiferal samples, and five additional aliquots of standard marble. The blank is fully processed and provides an estimate of the residual memory of the previous sample. The laboratory standard Carrara marble was calibrated to PDB through NBS 19, using the values -2.20‰ for $\delta^{18}\text{O}$ and +1.95‰ for $\delta^{13}\text{C}$, as recommended by Coplen (1988). Analytical reproducibility (as indicated by the marble analyses) typically was about $\pm 0.06\%$ ($1-\sigma$) for $\delta^{18}\text{O}$ and somewhat better for $\delta^{13}\text{C}$. Unfortunately, reproducibility does appear to be variable; presumably, reproducibility depends on the level of contamination in the vacuum lines, which may vary on a daily or weekly basis.

The strategy for treating "bad" measurements is seldom discussed, yet the appropriate strategy does depend both on the overall objectives and on the methods that are being used to achieve them. For example, if a conclusion is to be supported visually, it is appropriate to show "unacceptable" data with an indication that the eye should ignore them; on the other hand, numerical analysis should generally be performed on the best rendition of the data. If, as is the case with this research, time series analysis is to be applied, the objective of the measurements is to derive the most likely time series (of equilibrium calcite $\delta^{18}\text{O}$ and $\delta^{13}\text{C}$) for the location. The measurements of percentage of coarse fraction provide an example where alternative requirements are clear: were one presenting measurements to derive a time series for foraminiferal dissolution, one might prefer to screen the samples visually to eliminate coarse fraction estimates for samples containing volcanic ash or terrigenous sand; on the other hand, were one using these same data to seek ash layers or turbidites, one obviously would wish to use all these data.

Unfortunately, it is the case that on rare occasions, unacceptable numbers are output from the mass spectrometer; the following discussion outlines the procedure that we adopted when this was suspected. The easiest situation to deal with is when a whole sequence of samples has yielded aberrant values, and a clear malfunction in the system can be identified. In this case, these values are rejected outright and are not tabulated. A situation that arose during this work was that a valve near the freezing trap in the carbonate preparation line malfunctioned, which caused gases to fractionate isotopically during transfer; in this case, the entire run of analyses was rejected. Also, occasional measurements that were unacceptable because the quantity of carbon dioxide was insufficient for a reliable measurement were rejected outright.

Should an isolated sample deviate from the adjacent measurements in the sediment sequence, our practice was to re-pick the sample, ideally for more than one additional measurement. If the original measurement deviated both from the adjacent samples in the core and from two replicate analyses, we eliminated it from the mean. Measurements that have been rejected on this basis are tabulated, but have been marked. Sometimes, no useful specimens were available for a replicate measurement and, in this case, probably some compromise was necessary to obtain specimens for the first analysis, and thus, one may be justified in rejecting that first measurement, even though it cannot be replicated. Of 2765 $\delta^{18}\text{O}$ measurements tabulated, eight have been rejected; of these, one was in the top of a core (138-846B-21X-1, 45-47 cm) and clearly represents contamination.

This discussion clarifies the importance of achieving a close sampling density. Experience gained over many years shows that if one samples a deep-sea sediment sequence at intervals comparable with the bioturbation depth, the difference between successive samples is almost identical to the difference between replicate measurements in the same sample and thus provides the geologically best criterion by which to evaluate data reliability (Shackleton and Opdyke, 1973). Thus, if (but only if) the sequence is sampled this closely, one does have a statistical criterion by which to eliminate a single aberrant measurement. One may argue that statistical analysis is biased by such a procedure, but the fact is that in reality, not all variability is

distributed normally. For example, a mislabeled sample, a mental aberration whereby planktonic foraminifers were selected instead of benthic foraminifers, or a single, large reworked specimen might all give rise to a deviation from the expected measurement, whose probability cannot be predicted from the Gaussian distribution of the vast majority of deviations.

BIOSTRATIGRAPHY

The high quality shipboard biostratigraphy of Site 846 is given in the site chapter (Mayer, Pisias, Janecek, et al. 1992). In addition, we determined several foraminiferal datums while picking samples for isotope analysis. In view of the relatively small number of individual foraminifers in a 10-cm³ sample, by comparison with the three other microfossil groups, a considerable advantage can be gained from the opportunity to examine such a large number of samples. Many of the species extinction datums observed can be determined between adjacent samples; however, the reliability of an extinction datum that is based on the first downhole observation of one or two specimens of an extinct species can be assessed only by observing the consistency of its presence in subsequent samples down the section. Table 2 gives the foraminiferal biostratigraphic datums for Site 846 that we observed. The relationship of biostratigraphic events to the oxygen isotope stratigraphy is discussed in Shackleton et al. (this volume).

RESULTS

All analytical data are given in Table 3. In addition to the ODP conventional sample identifier, each sample has been assigned three depths. First is the conventional depth below seafloor, as estimated by the length of pipe and position in core; the conventional abbreviation "mbsf" (meters below seafloor) has been used. Second is "mcd" (meters composite depth), as derived aboard the ship by constructing a continuous composite section taking into account documented overlapping between several holes at the site (Hagelberg et al., 1992). Typically, mcd values exceed mbsf values by more than 10%, with the offset being by definition constant for each core in the hole. It is absolutely essential to use this adjustment to construct a continuous section for time series analysis. Third is "rmcd" (revised meters composite depth), which has been derived to take into account distortions within cores (Hagelberg et al., this volume). Differences between rmcd and mcd seldom exceed 20 cm in sediments recovered using the APC. Making these adjustments (which are based primarily on examination of the GRAPE density data), improves the continuity of the $\delta^{18}\text{O}$ values and is desirable if comparisons are to be made with time series of other parameters (such as GRAPE density), which are based on data not from Hole 846D. In all the discussion in the remainder of this chapter, "depth" may be taken to imply "rmcd," unless otherwise stated.

To illustrate and process the data in Table 3, adjustments were made to take into account taxon-dependent departures from isotopic equilibrium using the adjustment factors given in Table 4. Note that several taxa are regarded as unreliable with regard to $\delta^{13}\text{C}$, so that the final data set is somewhat more limited for $\delta^{13}\text{C}$ than for $\delta^{18}\text{O}$. Figure 1 shows the $\delta^{18}\text{O}$ measurements vs. depth. All individual measurements have been plotted, including data for overlapping intervals from different holes. To guide the eye, a line representing a Gaussian smoothing of the data has been drawn; this is for illustrative purposes only. Figure 2 shows the raw $\delta^{13}\text{C}$ data as a function of depth, similarly with a smooth line to guide the eye.

CHRONOLOGY

To develop a time series from the data shown in Figures 1 and 2, a few unreliable measurements were excluded and the remaining

Table 2. Foraminiferal biostratigraphic datums in Site 846.

Datum	Upper limit	Lower limit
<i>Globigerinoides fistulosus</i> LAD	846B 5/CC	846B 6/1/76
<i>Globorotalia limbata</i> LAD	846D 8/3/136	846D 8/3/146
<i>Globoquadrina altispira</i> LAD	846D 12/6/56	846D 12/6/66
<i>Globigerinoides fistulosus</i> FAD	846D 12/4/25	846D 12/4/106
<i>Sphaeroidinellopsis seminulina</i> LAD	846D 12/6/76	846D 12/6/86
<i>Pulleniatina spectabilis</i> LAD	846D 16/2/106	846D 16/2/116
<i>Globoquadrina dehiscentes</i> LAD	846D 20/6/36	846D 20/6/46

Note: LAD = last appearance datum; FAD = first appearance datum.

replicates in each sample averaged (see discussion above). In intervals where sampling led to overlapping between adjacent holes, the noisier of the two overlapping portions was eliminated unless the congruence was excellent. Table 5 gives the depth series that was used for the time series construction.

The age model for Site 846 that we use here is presented in Table 6. Its derivation is given in Shackleton et al. (this volume) in the context of age models for all the sites drilled during Leg 138. As shown in that chapter, it has been possible to construct age models by correlating GRAPE density (reflecting percentage of carbonate) to variations in Northern Hemisphere summer insolation, as computed by Berger and Loutre (1991). However, it is appropriate to point out here that although it is possible by examining Figure 1 to discern more-or-less regular cycles (which emerge as orbital tilt cycles) having a wavelength that averages a little under 2 m between the top of the $\delta^{18}\text{O}$ record and about 130 mcd, below this depth these cycles cannot easily be followed continuously. Thus, it would have been relatively straightforward to develop a time scale based only on the $\delta^{18}\text{O}$ record down to this point (about 16 tilt cycles below the Gauss/Matuyama boundary). Below that depth, patches are seen where the signal-to-noise ratio in the $\delta^{18}\text{O}$ record is so low that it is not always clear whether tilt cycles are being registered, so that tuning could not have been achieved reliably on the basis of the $\delta^{18}\text{O}$ record alone.

Shackleton et al. (this volume), show cross spectra of a stacked GRAPE density record for Sites 849, 850, and 851 vs. insolation at 65°N. The GRAPE density record for Site 846 and for the stacked record are shown in Figure 3, together with the age control points that were used to construct the time scale for Site 846. To validate the transfer of the time scale to Site 846, we show in Figure 4 cross spectra of GRAPE density for Site 846 vs. the stacked record of Sites 849, 850, and 851. For the interval 5 to 6 Ma, coherencies are poor and we regard the time scale for Site 846 as suspect in detail in that interval. A possible reason is that in this site the lowest part of the Pliocene was cored using the XCB, and the composite depth section may be imperfect.

For each of the time intervals (1.7–3, 3–4, and 4–5 Ma), coherency between the GRAPE density record of Site 846 and the stacked record is high in the precession band, and the phase spectrum is also flat at zero phase. This is to be expected because it is the characteristic amplitude modulation of the precession signal that helped us when tuning the GRAPE density records to the orbital signal. In each of the same intervals, the phase spectrum is also flat at zero phase across the obliquity frequency band. Although not unexpected, this might not necessarily have been the case. In the older intervals, the two spectra compared are broadly similar, but in the youngest interval, 1.7–3 Ma, Site 846 has significantly more power concentrated in the obliquity band. Note that even in this interval, the phase spectrum shows GRAPE density in phase with 65°N insolation in the obliquity band.

The age model discussed above was applied to the isotope data by interpolating linearly on "rmcd" depth between the control points. The isotope data are shown in Figures 5 and 6 after interpolating at 3 k.y. intervals and smoothing with a Gaussian filter. The data points plotted after averaging replicate measurements from the same sample. Gaps in the line show where no interpolated value is present because no valid measurement falls within the 8.99 k.y. smoothing window.

Table 3. Stable isotope data for Site 846.

Sample	Depth (mbsf)	Depth (mcd)	Depth (rmcd)	Sample (ident.)	Species (code)	$\delta^{18}\text{O}$ (raw)	$\delta^{13}\text{C}$ (raw)	$\delta^{18}\text{O}$ (adj.)	$\delta^{13}\text{C}$ (adj.)	$\delta^{18}\text{O}$ (used)
I38-846B-										
7H-1, 75-77	55.25	63.55	63.430	P92/1666	UVIG	3.82	-1.25	3.82	-0.35	3.82
7H-1, 85-87	55.35	63.65	63.528	P92/1667	UVIG	3.78	-1.31	3.78	-0.41	3.78
7H-1, 95-97	55.45	63.75	63.626	P92/1668	UVIG	3.42	-1.08	3.42	-0.18	3.42
7H-1, 105-107	55.55	63.85	63.725	P92/1669	UVIG	3.51	-1.13	3.51	-0.23	3.51
7H-1, 115-117	55.65	63.95	63.823	P92/1670	UVIG	3.59	-1.10	3.59	-0.20	3.59
7H-1, 127-129	55.77	64.07	63.941	P92/1671	PWUELL	2.76	-0.11	3.40	-0.11	3.40
7H-1, 135-137	55.85	64.15	64.027	P92/1672	ORID	3.84	-1.53	3.84	-0.53	3.84
7H-1, 145-147	55.95	64.25	64.150	P92/1673	UVIG	3.76	-1.28	3.76	-0.38	3.76
7H-2, 5-7	56.05	64.35	64.278	P92/1674	UVIG	4.09	-1.55	4.09	-0.65	4.09
7H-2, 13-15	56.13	64.43	64.387	P92/1675	UVIG	4.09	-1.43	4.09	-0.53	4.09
7H-2, 25-27	56.25	64.55	64.537	P92/1676	UVIG	4.03	-1.54	4.03	-0.64	4.03
7H-2, 35-37	56.35	64.65	64.650	P92/1677	UVIG	3.94	-1.52	3.94	-0.62	3.94
7H-2, 45-47	56.45	64.75	64.760	P92/1678	UVIG	4.10	-1.45	4.10	-0.55	4.10
7H-2, 55-57	56.55	64.85	64.860	P92/1679	UVIG	3.90	-1.29	3.90	-0.39	3.90
7H-2, 65-67	56.65	64.95	64.960	P92/1680	UVIG	3.90	-1.51	3.90	-0.61	3.90
7H-2, 77-79	56.77	65.07	65.080	P92/1681	UVIG	3.87	-1.47	3.87	-0.57	3.87
7H-2, 86-88	56.86	65.16	65.160	P92/1682	UVIG	3.69	-1.32	3.69	-0.42	3.69
7H-2, 95-97	56.95	65.25	65.250	P92/1683	UVIG	3.52	-1.17	3.52	-0.27	3.52
7H-2, 106-108	57.06	65.36	65.350	P92/1684	UVIG	3.60	-1.21	3.60	-0.31	3.60
7H-2, 115-117	57.15	65.45	65.440	P92/1685	UVIG	3.67	-1.26	3.67	-0.36	3.67
7H-2, 125-127	57.25	65.55	65.540	P92/1686	UVIG	3.59	-1.34	3.59	-0.44	3.59
7H-2, 135-137	57.35	65.65	65.650	P92/1687	UVIG	3.64	-1.16	3.64	-0.26	3.64
7H-2, 145-147	57.45	65.75	65.750	P92/1688	UVIG	3.53	-1.17	3.53	-0.27	3.53
7H-3, 15-17	57.65	65.95	65.960	P92/1690	UVIG	3.71	-1.41	3.71	-0.51	3.71
7H-3, 25-27	57.75	66.05	66.060	P92/1691	UVIG	3.60	-1.50	3.60	-0.60	3.60
7H-3, 35-37	57.85	66.15	66.160	P92/1692	UVIG	3.97	-1.58	3.97	-0.68	3.97
7H-3, 45-47	57.95	66.25	66.250	P92/1693	UVIG	4.00	-1.42	4.00	-0.52	4.00
7H-3, 55-57	58.05	66.35	66.350	P92/1694	UVIG	3.73	-1.44	3.73	-0.54	3.73
7H-3, 65-67	58.15	66.45	66.450	P91/2364	UVIG	3.43	-0.88	3.43	-0.02	3.43
7H-3, 65-67	58.15	66.45	66.450	P91/2365	PWUELL	3.08	-0.34	3.72	-0.34	3.72
7H-3, 77-79	58.27	66.57	66.560	P91/2366	UVIG	3.62	-1.09	3.62	-0.19	3.62
7H-3, 77-79	58.27	66.57	66.560	P91/2367	PWUELL	2.88	-0.24	3.52	-0.24	3.52
7H-3, 86-88	58.36	66.66	66.650	P91/2369	PWUELL	2.91	-0.30	3.55	-0.30	3.55
7H-3, 86-88	58.36	66.66	66.650	P91/2368	UVIG	3.52	-1.07	3.52	-0.17	3.52
7H-3, 95-97	58.45	66.75	66.740	P91/2370	PWUELL	2.77	-0.19	3.41	-0.19	3.41
7H-3, 106-108	58.56	66.86	66.850	P91/2371	UVIG	3.22	-1.07	3.22	-0.17	3.22
7H-3, 115-117	58.65	66.95	66.940	P91/2372	UVIG	3.51	-1.13	3.51	-0.23	3.51
7H-3, 124-126	58.74	67.04	67.030	P91/2373	UVIG	3.50	-1.20	3.50	-0.30	3.50
7H-3, 124-126	58.74	67.04	67.030	P91/2374	PWUELL	2.91	-0.19	3.55	-0.19	3.55
7H-3, 135-137	58.85	67.15	67.140	P91/2375	PWUELL	2.89	-0.04	3.53	-0.04	3.53
7H-3, 145-147	58.95	67.25	67.240	P91/2376	PWUELL	3.02	-0.02	3.66	-0.02	3.66
7H-4, 5-7	59.05	67.35	67.340	P91/2377	PWUELL	3.05	-0.22	3.69	-0.22	3.69
7H-4, 12-14	59.12	67.42	67.410	P91/2379	GLOBOBUL	3.98	-1.28	3.98	NA	3.98
7H-4, 12-14	59.12	67.42	67.410	P91/2378	PWUELL	3.06	-0.28	3.70	-0.28	3.70
7H-4, 24-26	59.24	67.54	67.520	P91/2380	PWUELL	2.96	-0.32	3.60	-0.32	3.60
8H-1, 25-27	64.25	74.45	74.301	P91/1791	UVIG	3.57	-1.14	3.57	-0.24	NA
8H-1, 34-36	64.34	74.54	74.360	P92/1792	UVIG	3.66	-1.15	3.66	-0.25	NA
8H-1, 45-47	64.45	74.65	74.450	P92/1793	UVIG	3.45	-1.15	3.45	-0.25	NA
8H-1, 55-57	64.55	74.75	74.620	P92/1794	UVIG	3.30	-1.10	3.30	-0.20	NA
8H-1, 65-67	64.65	74.85	74.805	P92/1795	UVIG	3.17	-1.29	3.17	-0.39	NA
8H-1, 75-77	64.75	74.95	75.010	P92/1796	UVIG	3.12	-1.02	3.12	-0.12	NA
8H-1, 86-88	64.86	75.06	75.250	P92/1797	UVIG	3.22	-0.91	3.22	-0.01	NA
8H-1, 95-97	64.95	75.15	75.340	P92/1799	UVIG	2.87	-1.04	2.87	-0.14	NA
8H-1, 105-107	65.05	75.25	75.393	P92/1800	UVIG	2.91	-1.13	2.91	-0.23	NA
8H-1, 115-117	65.15	75.35	75.440	P92/1801	PWUELL	2.49	-1.24	3.13	-1.24	NA
8H-1, 125-127	65.25	75.45	75.473	P92/1798	GLOBOBUL	3.24	-1.64	3.24	NA	NA
8H-1, 135-137	65.35	75.55	75.515	P92/1802	UVIG	3.45	-0.99	3.45	-0.09	NA
8H-1, 145-147	65.45	75.65	75.562	P92/1808	UVIG	3.11	-1.04	3.11	-0.14	NA
8H-2, 5-7	65.55	75.75	75.620	P92/1804	PWUELL	2.72	-0.17	3.36	-0.17	NA
8H-2, 5-7	65.55	75.75	75.620	P92/1803	UVIG	3.30	-0.97	3.30	-0.07	NA
8H-2, 15-17	65.65	75.85	75.700	P92/1805	PWUELL	2.55	-0.31	3.19	-0.31	NA
8H-2, 25-27	65.75	75.95	75.823	P92/1806	UVIG	3.33	-1.20	3.33	-0.30	NA
8H-2, 35-37	65.85	76.05	75.980	P92/1807	PWUELL	2.66	-0.36	3.30	-0.36	NA
8H-2, 46-48	65.96	76.16	76.157	P92/1809	UVIGLOB	3.50	-1.06	3.50	NA	NA
8H-2, 55-57	66.05	76.25	76.260	P92/1810	ORID	3.57	-1.27	3.57	-0.27	NA
8H-2, 65-67	66.15	76.35	76.355	P92/1811	UVIG	3.79	-1.09	3.79	-0.19	NA
8H-2, 78-80	66.28	76.48	76.470	P92/1812	PWUELL	2.78	-0.21	3.42	-0.21	3.42
8H-2, 85-87	66.35	76.55	76.537	P92/1813	PWUELL	3.03	-0.29	3.67	-0.29	3.67
8H-2, 94-96	66.44	76.64	76.633	P92/1814	UVIG	3.54	-1.29	3.54	-0.39	3.54
8H-2, 105-107	66.55	76.75	76.757	P92/1815	UVIG	3.34	-1.10	3.34	-0.20	3.34
8H-2, 115-117	66.65	76.85	76.850	P92/1816	UVIG	3.40	-1.46	3.40	-0.56	3.40
8H-2, 125-127	66.75	76.95	76.950	P92/1817	UVIG	3.18	-1.27	3.18	-0.37	3.18
8H-2, 135-137	66.85	77.05	77.060	P92/1818	UVIG	3.40	-1.48	3.40	-0.58	3.40
8H-2, 145-147	66.95	77.15	77.170	P92/1819	UVIG	3.53	-1.53	3.53	-0.63	3.53
8H-3, 5-7	67.05	77.25	77.270	P91/2381	UVIG	3.45	-1.21	3.45	-0.31	3.45
8H-3, 15-17	67.15	77.35	77.350	P92/1187	PWUELL	2.85	-0.86	3.49	-0.86	3.49

Notes: Each mass spectrometric measurement has a unique identification code: the letter P denotes a VG Isogas Prism mass spectrometer, and S denotes a VG Isogas SIRA Seris 9 mass spectrometer. This is followed by the two digits of the year and a four-digit run number which starts with 1 at the beginning of the calendar year. The species abbreviations are identified in Table 4 which also gives the adjustments made for each species. The final column repeats the $\delta^{18}\text{O}$ value for those samples that are used in the depth series in Table 5.

Only the first page of this table is reproduced here. The entire table appears on the CD-ROM (backpocket).

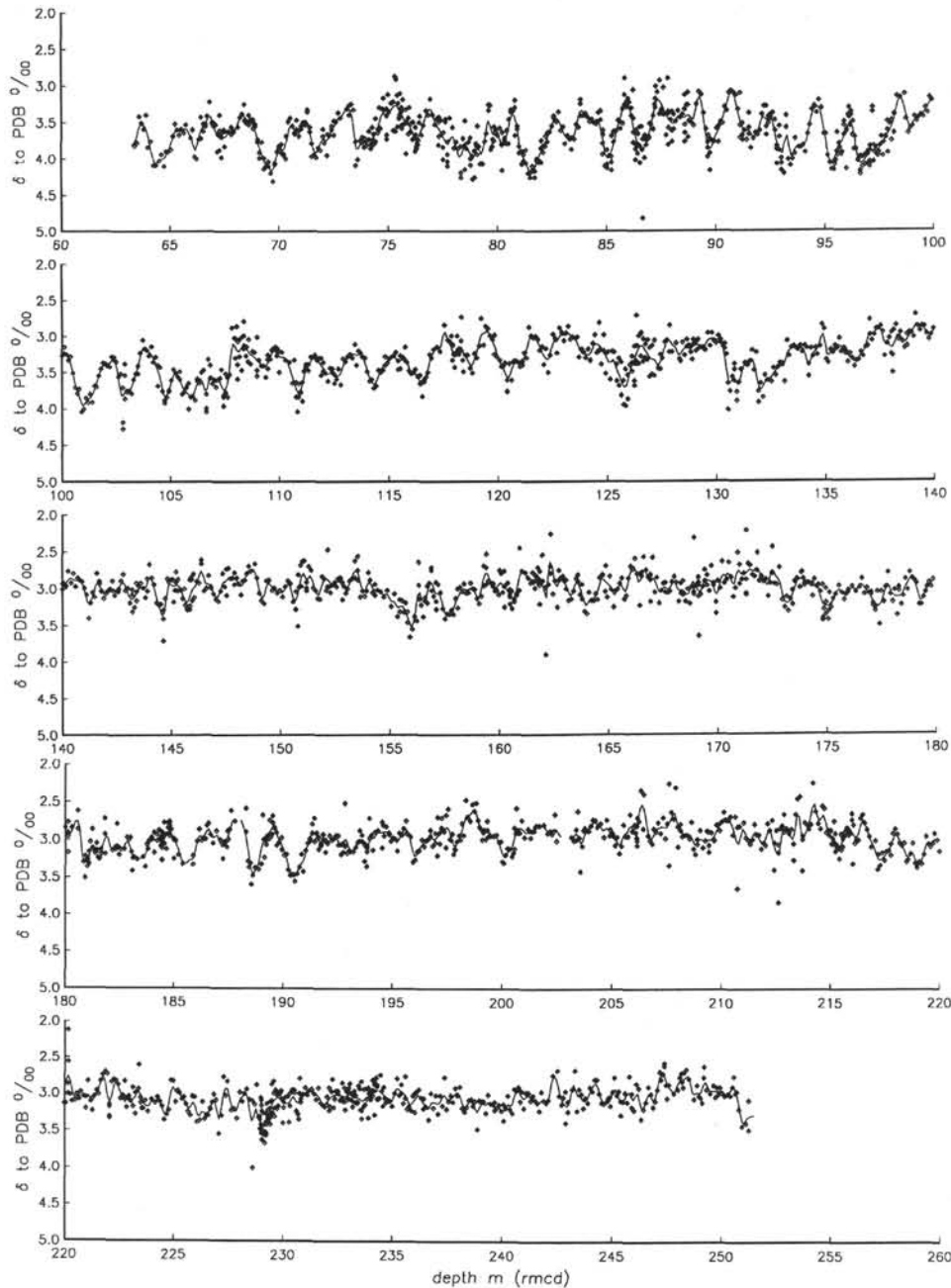


Figure 1. Oxygen isotope record for benthic foraminifers from Site 846 vs. depth rmcd. All data are shown; the line, a Gaussian interpolation at 10 cm with a 59.99 cm window, is solely to guide the eye.

OXYGEN ISOTOPE STAGES

Emiliani (1955) first devised the numerical scheme that is now almost universally used to designate successively older glacial and interglacial episodes indicated in the marine $\delta^{18}\text{O}$ record. This scheme was firmly codified by Shackleton and Opdyke (1973), when they showed that the record for the last several million years can reliably be taken as a global picture that is dominated by the effect of major fluctuations in the volume of ice on the northern continents.

Raymo et al. (1989) and Shackleton et al. (1990) erected a numerical scheme that extended to stage 104 at about the Gauss/Matuyama boundary and that had demonstrable utility in the sense that every one of these stages can be recognized clearly in both DSDP Site 607 in the Atlantic Ocean and ODP Site 677 in the Pacific Ocean. However, the difference between the benthic and planktonic records of Site 677 is

Table 4. Adjustment factors for $\delta^{18}\text{O}$, using *Uvigerina* as standard, and for $\delta^{13}\text{C}$, using *Cibicoides wuellerstorfi* as standard, applied to raw data in Table 3 before merging.

Abbreviation	Species	$\delta^{18}\text{O}$	$\delta^{13}\text{C}$
UVIG	<i>Uvigerina</i> sp.	0.00	0.90
HELEG	<i>Hoeglundina elegans</i>	-0.40	-1.30
PWUELL	<i>Cibicoides wuellerstorfi</i>	0.64	0.00
CIBKULL	<i>C. kullenbergi</i>	0.64	0.00
ORID	<i>Oridorsalis</i> sp.	0.00	1.00
GLOBOCAS	<i>Globocassidulina subglobosa</i>	-0.10	0.50
WUELKULL	<i>C. kull.</i> and <i>C. wuell.</i>	0.64	0.00
NUTT	<i>Nuttalides</i> sp.	0.35	0.00
NUTCIB	<i>Nuttalides</i> and <i>Cib.</i>	0.40	0.00
SBULL	<i>Sphaeroidina bulloides</i>	-0.10	-0.10
CIB	<i>Cibicoides</i> spp.	0.50	0.00
GYROID	<i>Gyroidina</i> sp.	0.00	0.00
GLOBOBUL	<i>Globobulimina pacifica</i>	0.00	NA

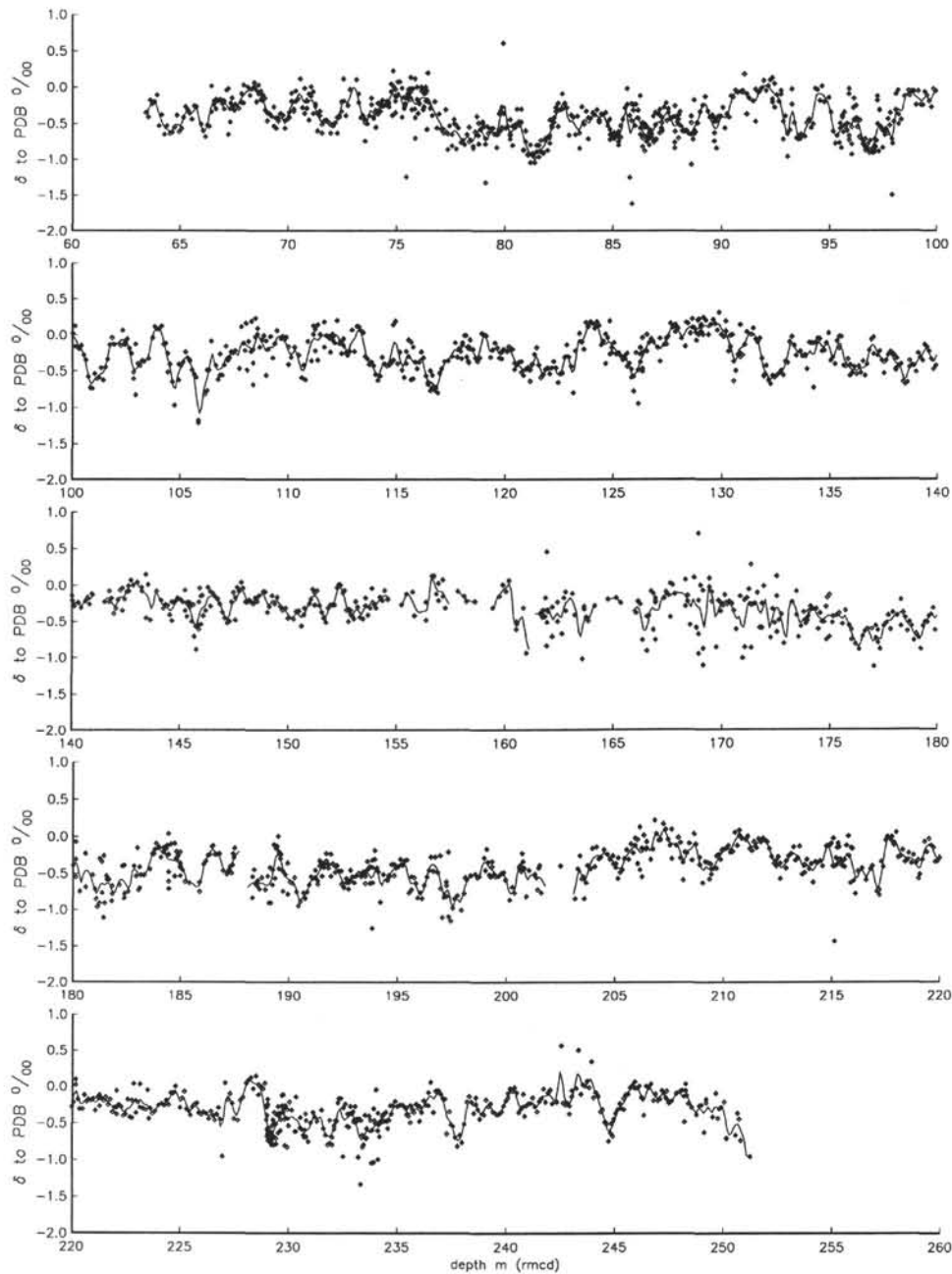


Figure 2. Carbon isotope record for benthic foraminifers from Site 846 vs. depth rmcd. All data are shown; the line (as Fig. 1) is to guide the eye.

so marked that the recognition of the isotope stages in the planktonic record is difficult. In parts of the record, it appears that the benthic record of Site 677 resembles the benthic record of Site 607 more closely than its own planktonic record. The reason for this may be that variability in deep-water temperature makes up a greater proportion of the overall $\delta^{18}\text{O}$ range in the Pliocene than in the Pleistocene. Thus, we recommend that the Pliocene isotope stages be regarded formally as being defined in a benthic $\delta^{18}\text{O}$ record.

Some scientists have extended the stage numbering scheme even farther; for example, Raymo et al. (1989) gave numbers to stage 116 at 2.73 Ma; Raymo et al. (1992) extended the numbering in Site 607 to 126; Sarnthein and Tiedemann (1989) gave numbers to stage 137 at about 3.3 Ma, and Tiedemann (1992) tentatively proposed numbers to stage 172 at almost 4.5 Ma. We consider that these numbers are

increasingly difficult to use effectively and that it may be more appropriate to erect a scheme analogous to that used by Hays et al. (1969) for Pacific Ocean carbonate cycles, whereby numbering restarts with each major change in magnetic field polarity. Hays et al. (1969) and Vincent (1981) used for carbonate cycles a scheme where numbering is re-initialized in each polarity chron. Because the records available today have higher resolution than those available in the late 1960s, we propose re-initializing at each magnetic polarity chron and subchron. Thus, we postulate that stage 105 becomes stage G1 (G for the section of Gauss to the Kaena; names of the form C3n. In $\delta^{18}\text{O}$.1 would be excessively clumsy but may become necessary if we extend the scheme into the Miocene). The cool stage that by counting downward in Site 846 would have been stage 126 becomes stage G22 in this new scheme. The preceding stage becomes

Table 5. Depth and age series used for time-series analysis.

Depth (mbsf)	Depth (rmcd)	Age (Ma)	$\delta^{18}\text{O}$	$\delta^{13}\text{C}$
55.25	63.43	1.763	3.82	-0.35
55.35	63.53	1.766	3.78	-0.41
55.45	63.63	1.769	3.42	-0.18
55.55	63.72	1.772	3.51	-0.23
55.65	63.82	1.776	3.59	-0.20
55.77	63.94	1.779	3.40	-0.11
55.85	64.03	1.782	3.84	-0.53
55.95	64.15	1.785	3.76	-0.38
56.05	64.28	1.789	4.09	-0.65
56.13	64.39	1.792	4.09	-0.53
56.25	64.54	1.796	4.03	-0.64
56.35	64.65	1.799	3.94	-0.62
56.45	64.76	1.802	4.10	-0.55
56.55	64.86	1.805	3.90	-0.39
56.65	64.96	1.807	3.90	-0.61
56.77	65.08	1.810	3.87	-0.57
56.86	65.16	1.813	3.69	-0.42
56.95	65.25	1.815	3.52	-0.27
57.06	65.35	1.818	3.60	-0.31
57.15	65.44	1.820	3.67	-0.36
57.25	65.54	1.823	3.59	-0.44
57.35	65.65	1.826	3.64	-0.26
57.45	65.75	1.829	3.53	-0.27
57.65	65.96	1.834	3.71	-0.51
57.75	66.06	1.836	3.60	-0.60
57.85	66.16	1.839	3.97	-0.68
57.95	66.25	1.841	4.00	-0.52
58.05	66.35	1.843	3.73	-0.54
58.15	66.45	1.845	3.58	-0.16
58.27	66.56	1.848	3.57	-0.22
58.36	66.65	1.850	3.54	-0.24
58.45	66.74	1.852	3.41	-0.19
58.56	66.85	1.855	3.22	-0.17
58.65	66.94	1.857	3.51	-0.23
58.74	67.03	1.859	3.53	-0.25
58.85	67.14	1.861	3.53	-0.04
58.95	67.24	1.864	3.66	-0.02
59.05	67.34	1.866	3.69	-0.22
59.12	67.41	1.868	3.84	-0.28
59.24	67.52	1.870	3.60	-0.32
59.25	67.56	1.871	3.73	-0.24
59.35	67.73	1.875	3.62	-0.29
59.45	67.85	1.878	3.61	-0.15
59.55	67.95	1.880	3.62	-0.10
59.75	68.15	1.884	3.56	0.00
59.85	68.25	1.886	3.43	-0.11
59.95	68.35	1.888	3.38	-0.02
60.05	68.45	1.890	3.36	0.04
60.15	68.55	1.892	3.51	-0.12
60.25	68.65	1.894	3.47	-0.03
60.35	68.75	1.896	3.47	-0.11
60.45	68.85	1.898	3.52	-0.14
60.55	68.95	1.900	3.54	-0.23
60.65	69.05	1.902	3.75	-0.41
60.75	69.15	1.904	3.95	-0.37
60.85	69.25	1.906	3.77	-0.40
60.95	69.35	1.908	4.07	-0.40
61.05	69.45	1.910	4.10	-0.49
61.15	69.55	1.912	4.07	-0.44
61.25	69.65	1.914	4.20	-0.36
61.35	69.75	1.916	4.31	-0.38
61.45	69.85	1.918	4.07	-0.51
61.55	69.95	1.920	3.90	-0.44
61.65	70.05	1.922	3.84	-0.38
61.75	70.15	1.924	3.86	-0.14
61.85	70.25	1.926	3.94	-0.32
61.95	70.35	1.928	3.85	-0.12
62.05	70.45	1.931	3.49	-0.16
62.15	70.55	1.933	3.44	0.12
62.25	70.65	1.935	3.55	-0.28
62.35	70.75	1.937	3.65	-0.19
62.45	70.85	1.939	3.54	-0.24
62.55	70.95	1.942	3.65	-0.27
62.65	71.05	1.944	3.57	-0.06
62.75	71.15	1.946	3.52	-0.21
62.85	71.25	1.948	3.52	-0.25

Notes: For each sample in the sequence the adjusted $\delta^{18}\text{O}$ and $\delta^{13}\text{C}$ measurements are averaged. Depth mbsf and rmcd are given with age derived using the age model of Table 6 (from Shackleton et al., this volume).

Table 6. Age model for the Pliocene and topmost Miocene section of Site 846 (from Shackleton et al., this volume).

Depth (rmcd)	Age (Ma)
0.00	0.000
1.80	0.039
3.70	0.088
5.96	0.127
6.76	0.148
7.38	0.171
7.94	0.184
8.76	0.220
9.60	0.240
9.94	0.247
11.04	0.278
11.26	0.290
11.84	0.310
12.36	0.326
12.66	0.333
13.44	0.354
15.04	0.388
15.70	0.405
16.26	0.422
17.06	0.446
18.78	0.479
19.90	0.509
20.14	0.515
20.38	0.523
20.96	0.544
22.12	0.579
22.88	0.614
23.38	0.628
24.42	0.659
25.38	0.681
25.72	0.692
26.26	0.717
26.92	0.737
28.16	0.772
28.74	0.783
32.18	0.863
33.26	0.884
34.34	0.908
35.14	0.936
35.98	0.978
36.56	0.999
37.46	1.029
37.92	1.050
39.80	1.092
40.80	1.114
42.12	1.136
44.68	1.215
45.14	1.243
47.12	1.317
47.74	1.337
48.86	1.358
49.54	1.379
50.64	1.400
52.14	1.431
53.06	1.473
53.58	1.493
54.58	1.513
54.92	1.528
55.22	1.547
55.80	1.567
57.24	1.606
58.28	1.645
59.18	1.664
60.96	1.697
61.72	1.708
64.02	1.782
65.88	1.832
67.72	1.875
70.24	1.926
71.20	1.947
72.36	1.968
73.62	1.986
74.88	2.023
79.00	2.086
79.50	2.097
80.06	2.118
80.74	2.140
82.60	2.190
83.88	2.211

Only the first page of this table is reproduced here. The entire table appears on the CD-ROM (backpocket).

Only the first page of this table is reproduced here. The entire table appears on the CD-ROM (backpocket).

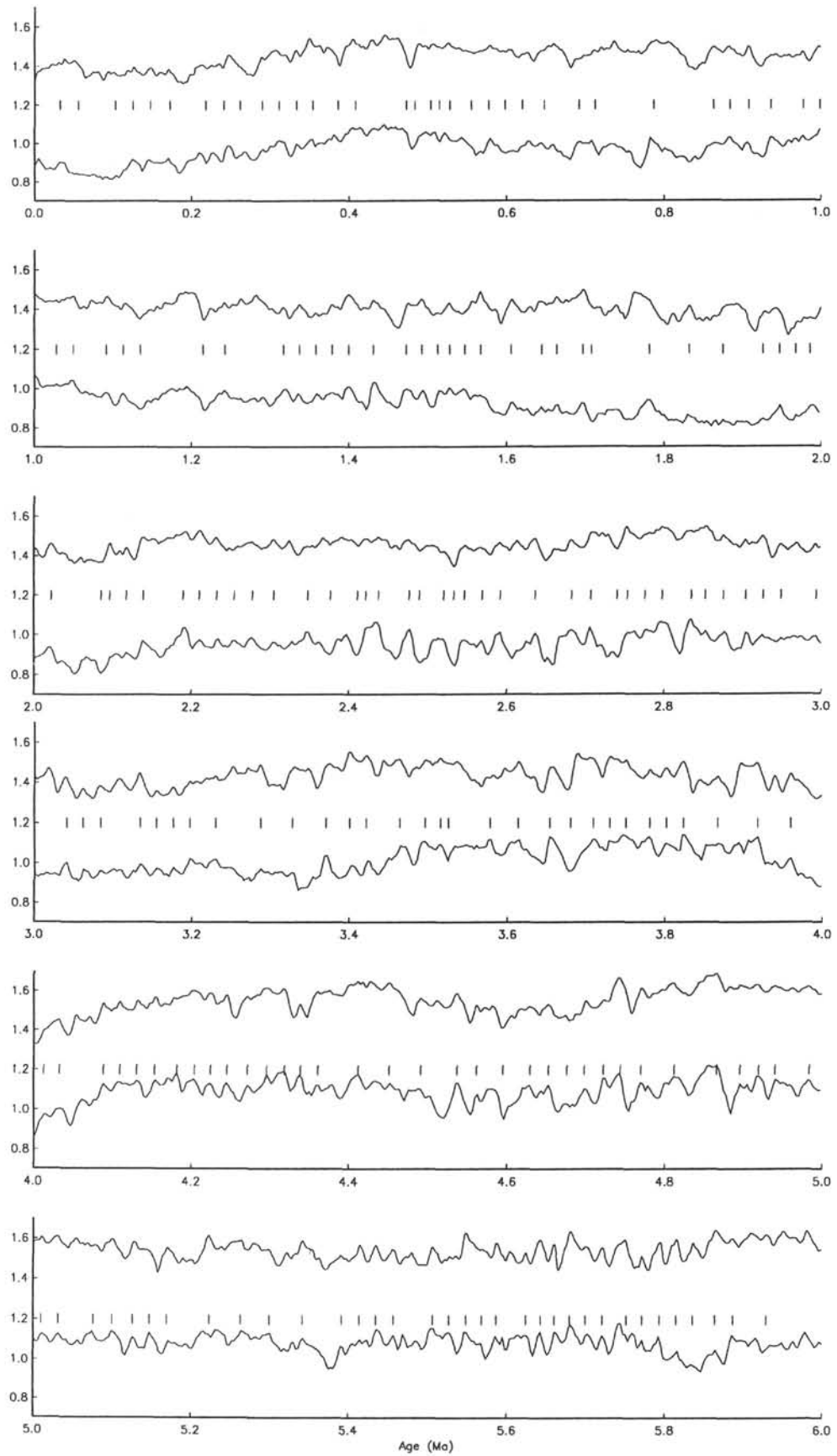


Figure 3. GRAPE density record of Site 846 (below, offset scale) compared with a stacked GRAPE density record for Sites 849, 850, and 851 (above, from Shackleton et al., this volume). Vertical lines show the age control points on the record for Site 846.

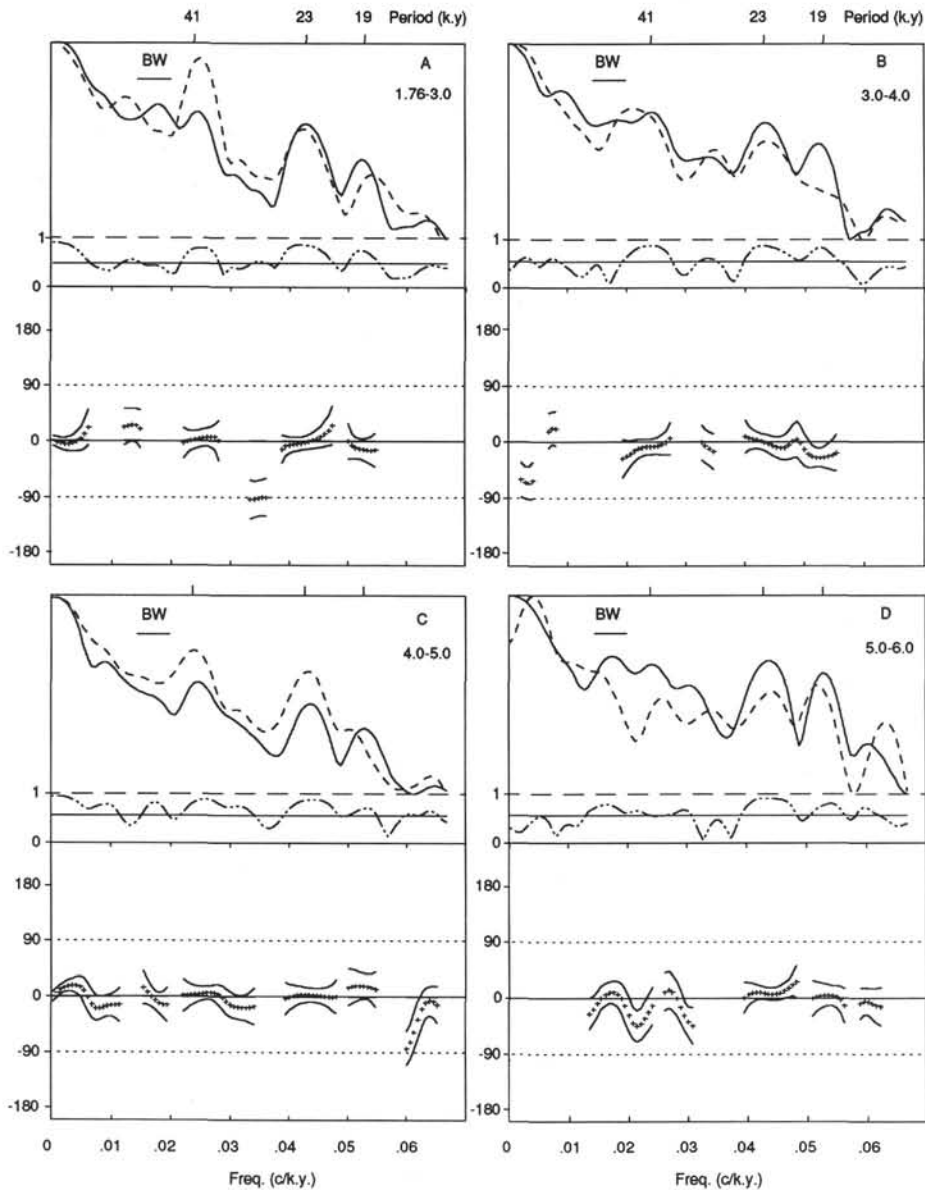


Figure 4. Cross-spectral analyses of the GRAPE density record of Site 846 (dashed line) vs. a stacked GRAPE density record of Sites 849, 850 and 851 (solid line, from Shackleton et al., this volume). **A.** 1.76 to 3 Ma. **B.** 3 to 4 Ma. **C.** 4 to 5 Ma. **D.** 5 to 6 Ma. In each panel, variance is shown on a log scale; the lowest line (dashed/dotted) shows coherence with the 80% confidence limit. Phase estimates have been plotted only where coherence is significant.

stage K1 (without prejudging the precise position of the top of the Kaena, but making the arbitrary decision that in order for each new series to count down from a warm stage 1 at the top, the lowest stage in the series above must be an even-numbered cold stage).

The value of reorganizing the nomenclature becomes clear should one attempt to use the scheme of Sarnthein and Tiedemann (1989); in their Figure 6, they indicated the top of the Kaena in stage 122 in Site 606 and in stage 126 in Site 552A and implicitly in stage 124 in Site 658. It is not clear to the detail of a single stage how these sites should be correlated at that point. By the level of the base of the Gauss, we might define 150 stages, whereas Tiedemann (1992) defined only 140; yet the glacial stage he named stage 142 can be unequivocally recognized in the record of Site 846; we re-designated this as stage Gi2. Thus, careful use of this scheme avoids cumulative uncertainties.

We have aimed not to define more stages than appears useful, bearing in mind that the purpose of the exercise is communication; should further subdivision be required in the future for either discussion or for correlation purposes, lettered substages analogous to 5a to 5e in the late Pleistocene may be used.

The data from Figure 5 are shown with isotope stage numbers and a magnetostratigraphy in Figure 7. The magnetostratigraphy was developed in Sites 850 and 851 (for the Gauss) and Site 852 (for the Gilbert). Correlation between Site 846 and these other sites has been based on tuning each of the GRAPE density records to the orbital insolation record of Berger and Loutre (1991), as discussed in Shackleton et al. (this volume). Note that the time scale shown here for the magnetostratigraphy is the one developed by Shackleton, Berger, and Peltier (1990), henceforth SBP90, and by Shackleton et

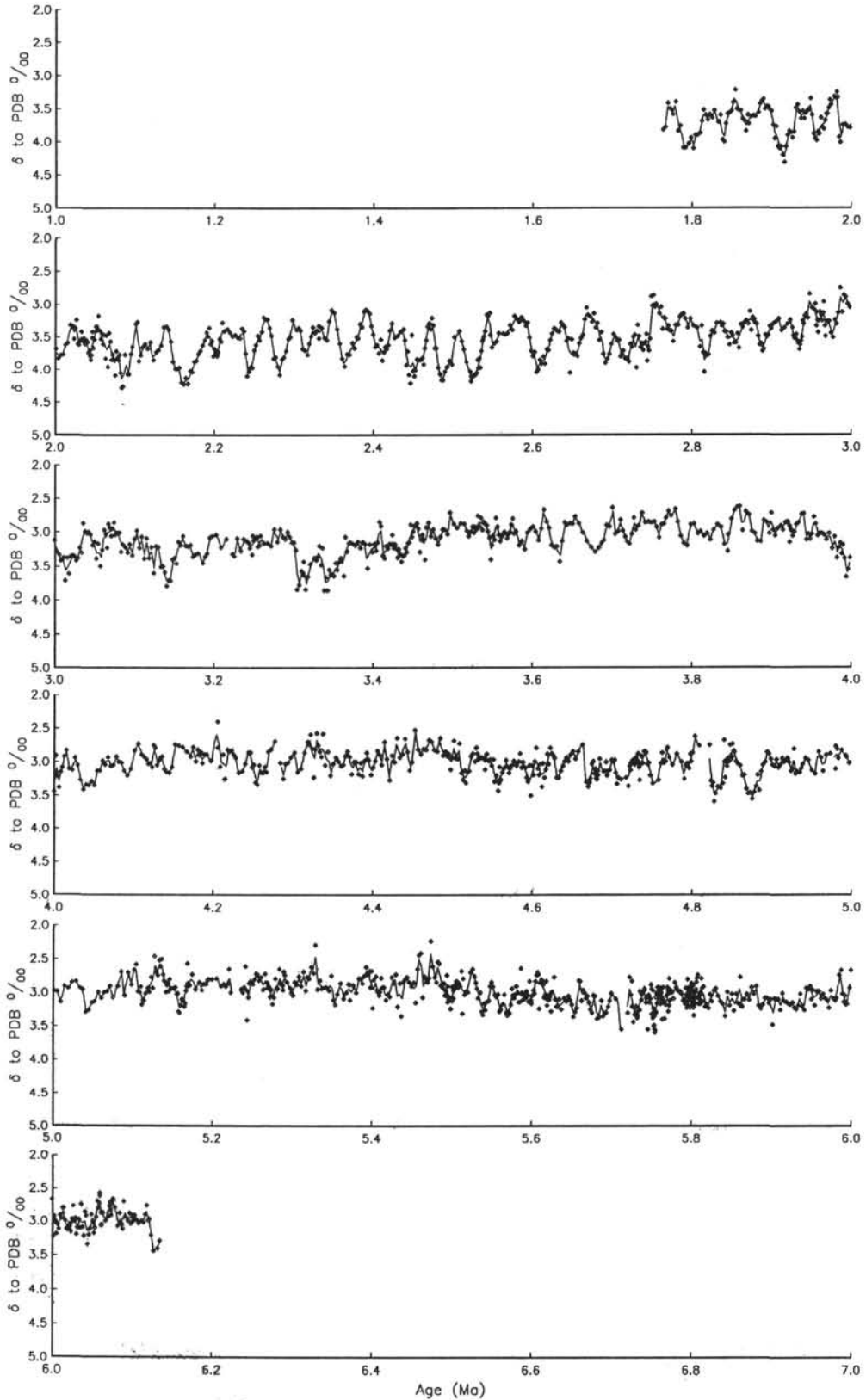


Figure 5. Oxygen isotope record from Site 846 vs. age. The line shows an interpolation at 3-k.y. intervals smoothed using a Gaussian filter having a total width of 8.99 k.y. The data points show the average where replicate analyses were made in the same sample. Gaps in the line show where no measurement falls within the interpolation window; note that the time series analysis was performed using a narrower smoothing window than that used for this figure.

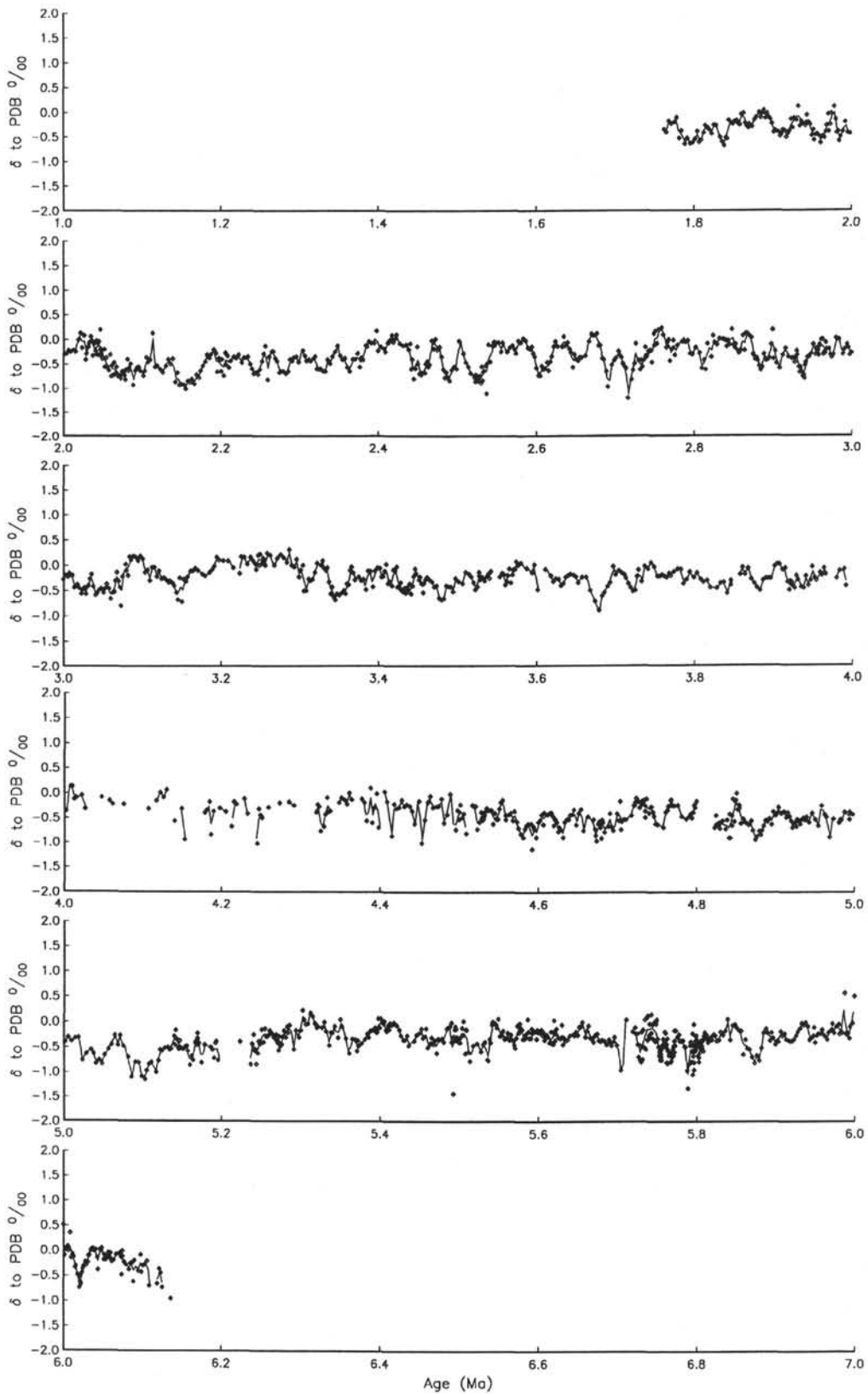


Figure 6. Carbon isotope record from Site 846 vs. age, generated as Figure 5.

al. (this volume), henceforth referred to as SCHPS94. This time scale is significantly different from those used over the past few years (e.g., Berggren et al., 1985), having ages typically 5% to 7% older.

From the base of the Pleistocene to stage 104, the stage numbers in Figure 7 are as used by Raymo et al. (1989) and by Shackleton et al. (1990). Stage G1 is equivalent to stage 105 of Raymo et al. (1989). It appears from an examination of Raymo et al. (1992, their Fig. 3A) that our numbering is equivalent on a one-to-one basis to theirs for DSDP Site 607, with our G22 being their 126 immediately above the Kaena.

In this scheme, the Kaena includes only two stages: stage KM1 straddles the base of the Kaena and stage KM6 straddles the top of the Mammoth. Again, the Mammoth includes only two stages, with MG1 straddling its base. In this interval, cool stages KM2, M2, and GM2 attain $\delta^{18}\text{O}$ values similar to those of the cool stages in the upper Gauss. The $\delta^{18}\text{O}$ signal in the lower part of the Gauss is of low amplitude, and it is difficult to subdivide it in great detail on the basis of the Site 846 record.

From the top stage of the Gilbert to the Cochiti, we defined stages Gi1 to Gi22. Within the Cochiti, there is a clear cool extreme that we call Co2, but it is not clear whether further subdivision is warranted. Between the Cochiti and the Nunivak, we defined a clear, warm CN1 and a broad, cool CN2; stage N1 straddles the top of the Nunivak, which is characterized by regular cycles N2 to N6. These more-or-less regular cycles continue as NS1 to NS8 and S1 to S16. Between the Sidujfall and the Thvera, we recognized two stages, while the Thvera includes stages T1 to T8. Stage TG1 is almost entirely within the Thvera, below which we defined stages to Stage TG24.

TIME-SERIES ANALYSIS

Time-series analysis was performed in million-year intervals using standard methods (Jenkins and Watts, 1968) on the data shown in Figures 5 and 6. Those data have been interpolated at 3-k.y. intervals by using a Gaussian weighting filter (Shackleton and Imbrie, 1990) with a total width 5.99 k.y. (this is narrower than the window used for Figures 5 and 6). This interpolation method inserts a gap code (-9999.00) at each age point for which no data are available within the window. The time series analyzed is given in Table 7. In the age interval 1.8 to 6.0 Ma, 72 points are missing in the $\delta^{18}\text{O}$ record (about 5% of the record). For the $\delta^{13}\text{C}$ record, the situation is much less favorable. The 4 to 4.4 Ma interval was not analyzed because more than half of the data points are missing; in the rest of the record, there are 120 gaps (about 10%).

Cross spectra of $\delta^{18}\text{O}$ vs. insolation at 65°N are shown in Figure 8. For these analyses, the sign of $\delta^{18}\text{O}$ was reversed, just as the data are, following the convention established by Emiliani (1955), plotted with lighter values upward, because more negative $\delta^{18}\text{O}$ values are associated with warmer climate. Figure 8A covers the interval from 1.7 to 3.0 Ma. Coherency in the obliquity bandwidth is high, and there is a marked concentration of variance seen in this band. There is no well-marked concentration of variance in the precession band. $\delta^{18}\text{O}$ (reversed) lags insolation in the obliquity bandwidth by about 50°. In the 3 to 4 Ma interval (Fig. 8B), the result is similar. Again, $\delta^{18}\text{O}$ variability is concentrated in the obliquity bandwidth, with high coherency and a lag of about 80° against insolation. In the interval 4 to 5 Ma (Fig. 8C), there is again only significant coherency between $\delta^{18}\text{O}$ and insolation in the obliquity band; the overall spectrum is similar to the spectrum of insolation at 65°N, but this is probably an illusion (in view of the low coherency). In the interval from 5 to 6 Ma (Fig. 8D), there is no concentration of power at orbital frequencies. In view of the visual character of the record, this is not altogether surprising; the signal is noisy, irregular, and of low amplitude.

Figure 9 shows cross-spectral analysis for the $\delta^{13}\text{C}$ data. Figure 9A covers the interval from 1.7 to 3 Ma. A well-marked spectral peak can be observed at the obliquity frequency that is highly coherent. At the obliquity frequency, $\delta^{13}\text{C}$ lags insolation at 65°N by about 50°. This confirms that isotopically lighter $\delta^{13}\text{C}$ values are associated with

more positive $\delta^{18}\text{O}$ values (more glacial ice and/or colder deep water), as is the case in the Pleistocene (Shackleton and Pisias, 1985). In the interval from 3 to 4 Ma (Fig. 9B), $\delta^{13}\text{C}$ is again coherent with 65°N insolation in the obliquity bandwidth, again with a lag of about 50°. Because of the large number of gaps in the interval 4 to 4.4 Ma, this part was not analyzed by cross-spectral analysis. Instead, we examined only the interval 4.4 to 5 Ma (Fig. 9C) but in contrast with Fig. 8C, no coherency is present despite the spectral peak in the obliquity band. In the 5 to 6 Ma (Fig. 9D) interval, where the data cover is good, the absence of coherent power in the obliquity band may be a real feature of the record.

DISCUSSION

The Messinian

The question of the possible influence of glacial events during the latest Miocene on the isolation of the Mediterranean Sea has been aired many times; Kastens (1992) reviewed the question carefully. Kastens discussed the evidence for a glacial event early in the Gilbert that may have directly caused the final isolation of the Mediterranean. In the record of Site 846, the $\delta^{18}\text{O}$ data show a clear pair of glacial stages, TG20 and TG22, near the top of the Miocene. During the Gilbert, the only other glacial events of comparable magnitude were those at stages Si4 and Si6, between about 4.8 and 4.9 Ma; more positive glacial events were not observed again before the upper part of the Gauss. Keigwin (1987) gave an age of about 5.3 Ma for the glacial event discussed by Kastens (1992); our age of 5.75 Ma for TG22 is equivalent to 5.22 Ma on the time scale of Berggren et al. (1985), very close to Keigwin's age estimate. Clearly, this was indeed a globally significant event, strengthening the arguments put forward by Kastens (1992) for its having caused the final isolation of the Mediterranean. Whether it was truly a glacial event with the sea-level implication required by Kastens (1992), depends partly on the validity of arguments for a measure of deglaciation on Antarctica during late Miocene and Pliocene time. If these arguments are accepted, the magnitude of the fall in sea level at the base of stage TG22 could have been on the order of 50 m.

The Miocene/Pliocene Boundary

Hilgen (1991) gave an astronomically calibrated age for the base of the Pliocene (as defined by the base of the Trubi in Sicily) of 5.32 Ma. His estimate is based on a short extension of the astronomical calibration below the base of the Thvera. Because we obtained an identical estimate as Hilgen (1991) for the age of the base of the Thvera, a correlation between the base of the Trubi in Sicily and stage TG5 should be accurate to the resolution of the stages, as indicated in Figure 7.

Kastens (1992) suggested that a relatively extreme interglacial event associated with a rise in sea level might be expected to have created the inflow of open marine water that marked the base of the Pliocene. In Site 846, stage TG9 at an age of about 5.46 Ma is a more significant interglacial event than stage TG5. This suggests that the association of the most extreme interglacial of the lower Gilbert with the base of the Trubi in Sicily may be incorrect and, therefore, that its association with the final relinking of the Mediterranean with the open ocean is unproven. However, it does remain possible that either (1) the main cycles recognized in the basal part of the Trubi are associated with obliquity, in which case the base of the Trubi would correlate to about the position of the interglacial at 5.46 Ma; (2) sedimentation of the Trubi in Sicily did not start until about 100 k.y. after the open-ocean connection was resumed; (3) there was not enough erosion of the sill where the first connection to the open ocean was re-established at 5.46 Ma to prevent renewed desiccation during the next couple of glacial extremes, or (4) that the erratic data in stage TG9 are misleading and it was not characterized by significantly isotopically lighter $\delta^{18}\text{O}$ values than stage TG5, or finally (6) our

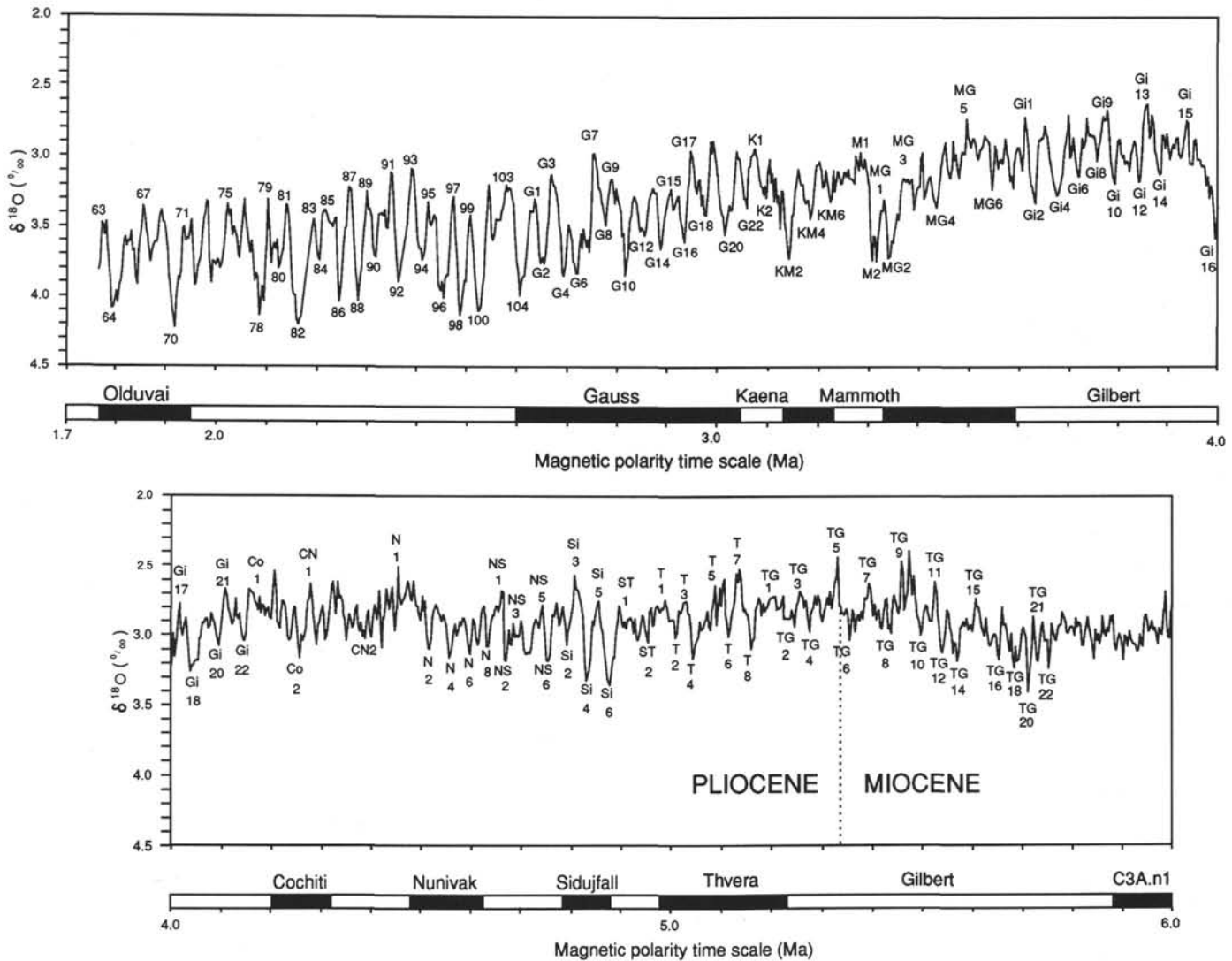


Figure 7. Oxygen isotope record from Site 846 vs. age, from Fig. 5. Proposed isotope stages are indicated. Above: 1.7 to 4 Ma. Below: 4 to 6 Ma. Below each panel is magnetic polarity history on the time scale used here.

correlations between Site 846 and the magnetostratigraphy of Site 852 may be weak in this time interval. Alternative 1 is unlikely in view of the convincing association between lithological cycles and precession during the whole of the Pliocene (Hilgen, 1991). Regardless of the precise correlation, the general trend in both glacial and interglacial extremes supports the notion that glacio-eustatic sea level may have exerted a major control over the timing of the base of the Pliocene, as well as over the Messinian desiccation event.

The Mid-Pliocene and Antarctic Deglaciation

The upper panel of Figure 10 shows the oxygen isotope record for the interval 2.5 to 3.5 Ma, marked with a horizontal line indicating the approximate δ¹⁸O value to be expected under present-day conditions, and a second line 0.9‰ lighter, a likely value were the Antarctic and Greenland ice sheets not present, and deep water temperature was the same as today. Turning first to the glacial extremes, we observed a remarkable and almost linear trend in the glacial value from stage G22 to stage 100. This re-enforces the deficiency of the record of Hole 552A, which Shackleton and Hall (1984) assumed to be continuous, but which probably contains a hiatus in the top part of the Gauss, having the effect of over-emphasizing the suddenness of the appearance of glacial stage 100 (Loubere and Moss, 1986). Although this

linear trend is an interesting description of the interval from 3.2 to 2.5 Ma, it does not, of course, have any relevance to the earlier Pliocene, during which no obvious trend in glacial values can be seen.

Turning now to the interglacial values, we see that during the latest Pliocene, between about 2.9 and 1.9 Ma, the predominant interglacial extreme value is close to the estimated value for today. Pending a careful evaluation of data from several sites, we suggest that there is no significant difference between them. An attempt to evaluate differences between interglacial extremes in the mid-Pleistocene (Shackleton, 1987) showed that it would be difficult to make meaningful distinctions between interglacial values at the 0.2% level on the basis of data from a single core.

At interglacial stage G17, we enter a new mode where the interglacial values are consistently at least 0.4‰ isotopically lighter than the present-day line. Indeed, with the exception of stages M2 and MG2, the predominant glacial value is close to the present-day line. Sarnthein and Fenner (1988) described the interval prior to our stage MG2 as the “Late Tertiary ‘golden age’ of stable climate,” an unfortunate concept that has led some people to think that the present man-induced rise in atmospheric carbon dioxide should be left unchecked so as to return Earth to this ‘golden age’ speedily. The interval in question is discussed in this context in Houghton, Jenkins, and Ephraums (1990, pp. 203–204). Our data exhibit no evidence that

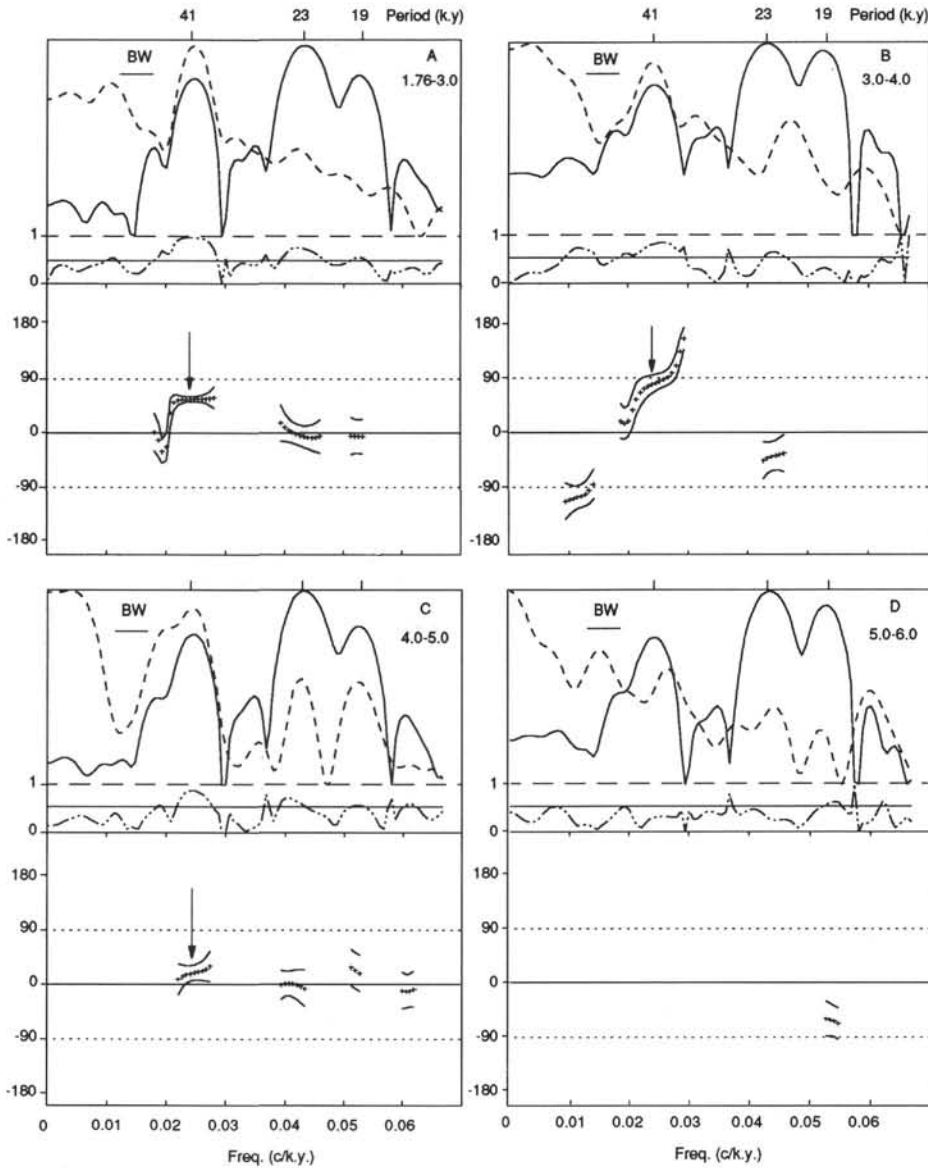


Figure 8. Cross spectral analyses of $\delta^{18}\text{O}$ record from Figure 5 (dashed line) vs. insolation at 65°N (solid line, data from Berger and Loutre, 1991). **A.** 1.76 to 3 Ma. **B.** 3 to 4 Ma. **C.** 4 to 5 Ma. **D.** 5 to 6 Ma. In each panel, variance is shown on a log scale; the dashed/dotted line shows coherence with a line at the 80% confidence limit. A positive phase implies that low ice-volume/high temperature lags high insolation. Phase estimates are plotted only where coherence is significant; heavy arrows show meaningful phase estimates in the obliquity band.

climate was stable in that interval. With regard to the nature of the variability, considerable uncertainty remains.

The lower panel in Figure 10 shows $\delta^{18}\text{O}$ data for the interval from 3.5 to 4.5 Ma, again with lines representing today's conditions and that expected with no Antarctic ice. One may interpret the observation that the typical range in benthic $\delta^{18}\text{O}$ is from 2.7‰ to 3.2‰ in terms of two possible contributions. First, one may assume that the volume and isotopic composition of the Antarctic ice sheet has been more or less constant since it formed during the mid-Miocene, in which case the variability in $\delta^{18}\text{O}$ implies that the temperature of the deep Pacific Ocean varied over a range of about 2°C . This interpretation goes back to the fundamental contributions of Kennett, Houtz, et al. (1974) during DSDP Leg 29. Second, one may assume that the temperature of the deep Pacific Ocean remained constant and that the fluctuations in $\delta^{18}\text{O}$ result from variations in the volume of ice stored on Antarctica. This second possibility has been the subject of considerable controversy in

recent years, exemplified by two reviews having identical titles, but taking opposite stances (Clapperton and Sugden, 1990; Webb and Harwood, 1991). The most important, and indeed dramatic, evidence in favor of glacial/interglacial cycles on the Antarctic continent is that extracted from the Sirius Group. Sediments in the Sirius Group contain undisputed in-situ fossils of *Nothofagus* (the southern beech) that are claimed on the basis of marine diatoms to be no older than late Pliocene. The marine diatoms themselves have been interpreted as implying that at some time no earlier than the beginning of the Pliocene a major marine incursion into central Antarctica occurred.

Among the varied evidences that have been adduced vs. this hypothesis is the deep ocean $\delta^{18}\text{O}$ record (Hodell and Venz, 1992). Although our record has a somewhat higher resolution than that generated by Hodell and Venz (1992), it contributes nothing new regarding the range of variability; we agree with them that the lowest $\delta^{18}\text{O}$ values are only about 0.6‰ to 0.7‰ lighter than today's values

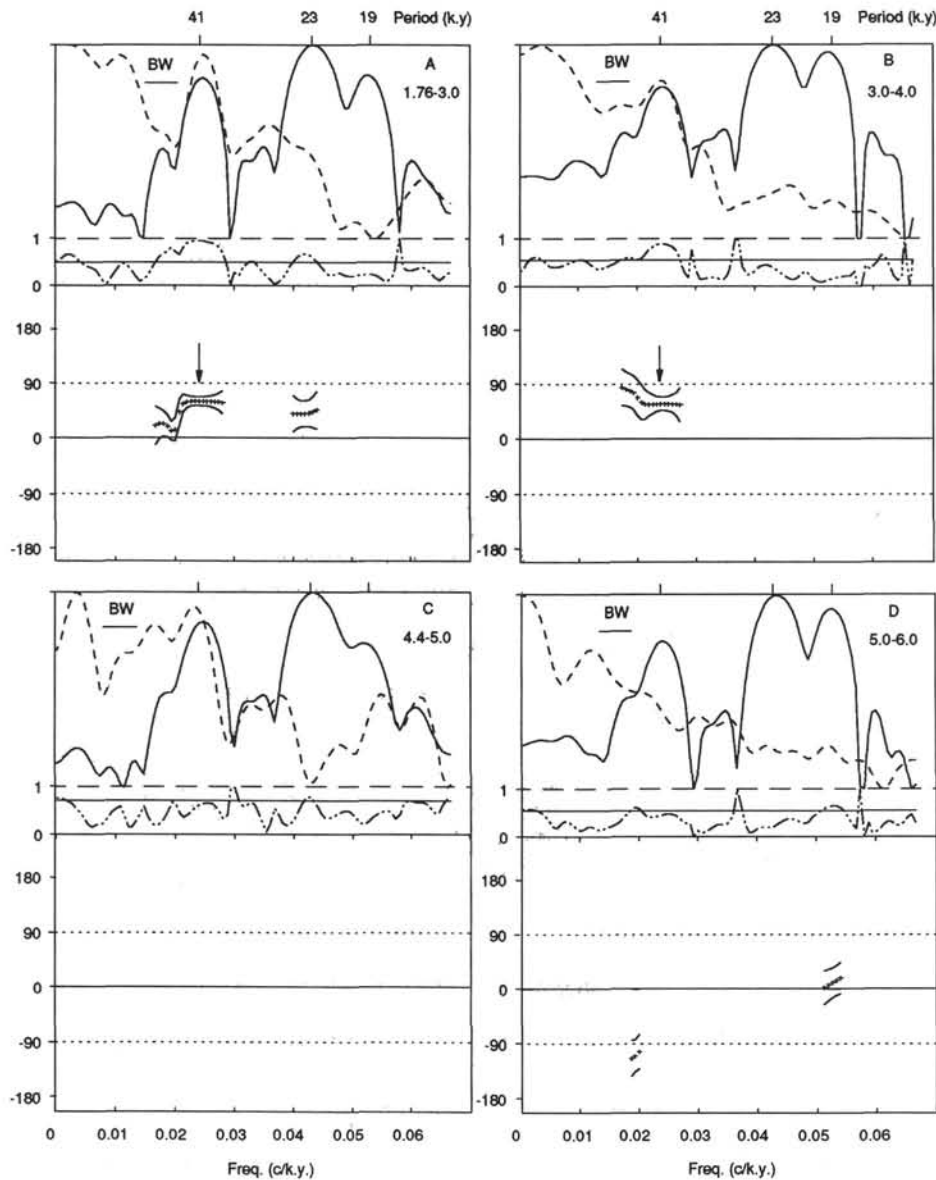


Figure 9. Cross-spectral analyses of $\delta^{13}\text{O}$ record from Figure 6 (dashed line) vs. insolation at 65°N (solid line, data from Berger and Loutre, 1991). **A.** 1.76 to 3 Ma. **B.** 3 to 4 Ma. **C.** 4.4 to 5 Ma. **D.** 5 to 6 Ma. In each panel, variance is shown on a log scale; the dashed/dotted line shows coherency with a line at the 80% confidence limit. Phase estimates are only plotted where coherency is significant; heavy arrows show meaningful phase estimates in the obliquity band.

(Fig. 10). This value does not permit total deglaciation of Antarctica and only permits major decreases in Antarctic ice volume, if these were accompanied by deep ocean temperatures no warmer than those of today. However, spectral analysis of our data does make a new contribution. Figure 8 shows a cross-spectral analysis of $\delta^{18}\text{O}$ vs. insolation at 65°N . At the period of obliquity variation, a well-defined phase lag of $82 \pm 9^\circ$ is seen for 3 to 4 Ma. In itself, this lag estimate should be treated with great caution, because of the inherent uncertainty in the exact relationship between precession and obliquity cycles in the older part of the record presented by Berger and Loutre (1991). A more robust estimate is that of the phase relationship between GRAPE density and $\delta^{18}\text{O}$ in the same core. Figure 11 shows cross spectra of GRAPE density in Site 846 vs. $\delta^{18}\text{O}$ in Site 846. Figure 11 shows that in the interval 3.5 to 4.5 Ma, illustrated in Figure 10A, the $\delta^{18}\text{O}$ spectrum is still significantly different from the GRAPE

density spectrum, with proportionally more power in the obliquity band. Figure 11 also shows that between 3.5 and 4.5 Ma, there was still a significant phase lag of (negative) $\delta^{18}\text{O}$ behind GRAPE density, implying that a significant component of the climate system still responded with a long time constant. A large ice sheet has to be regarded as the first candidate as a component of the climate system that has such a long time constant, and the figure estimated seems consistent with a fluctuating Antarctic ice sheet. Of course, we cannot exclude the possibility that the long time constant arises from some aspect of the operation of the global carbon system. However, we postulate that the most plausible explanation for the results presented is that during most of the Pliocene, the equatorial Pacific Ocean carbonate system responded directly to orbital forcing (presumably through atmospheric circulation changes), while in high southern latitudes, the Antarctic ice sheet underwent cyclic fluctuations forced

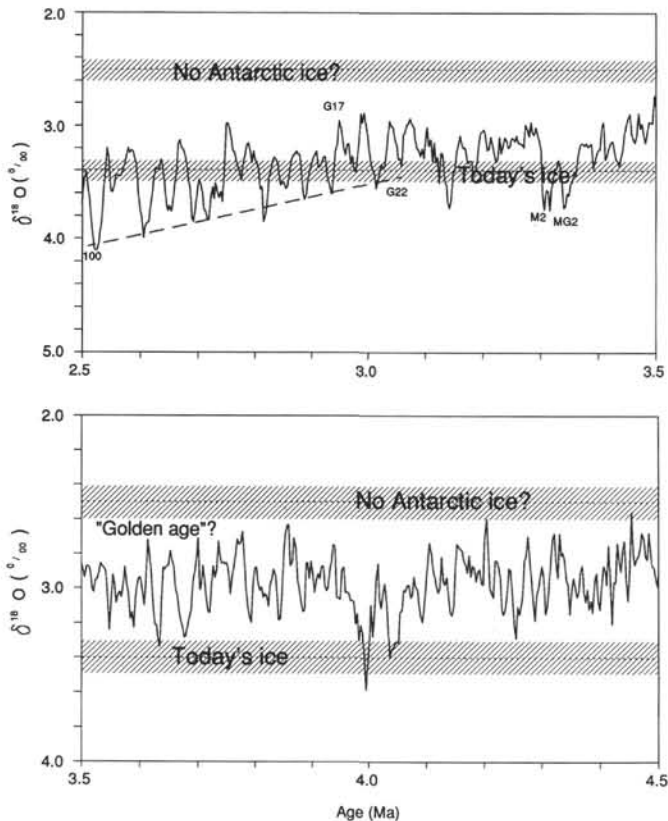


Figure 10. Oxygen isotope record of benthic foraminifers in Site 846 vs. age, compared with range expected under today's conditions and with no change other than returning the ice presently stored in Antarctica and Greenland to the ocean. Above: 2.5 to 3.5 Ma. Below: 3.5 to 4.5 Ma.

by obliquity variations (period about 41 k.y.) to exhibit a significant phase lag, such as one might expect for a continental-scale ice sheet. We draw attention in particular to the interval from 3.5 to 4.5 Ma, because in this interval, the $\delta^{18}\text{O}$ values are almost entirely lower than present-day values, so that any phase lag cannot readily be explained by variations in global ice volume above the present total, excluding Northern Hemisphere ice sheets from consideration. Hodell and Venz (1992) drew attention to the fact that the $\delta^{18}\text{O}$ fluctuation can be interpreted only in terms of Antarctic glacial cycles if ocean deep water remained very cold. The production of an ocean bottom water of 0°C does not absolutely require an ice sheet extending to the continental margin and generating ice shelves; on the other hand, it may require conditions that are inconsistent with the postulated vegetation. The field evidence against a temperate interval during the Pliocene is also strong (Marchant et al., 1993). Thus, it seems most likely that the $\delta^{18}\text{O}$ fluctuations shown in Figure 10 in reality reflect a combination of small variations in Antarctic ice volume and associated variations in deep water temperature.

CONCLUSIONS

An oxygen isotope stratigraphy for the entire Pliocene section of Site 846 has been constructed with an average sampling interval of less than 3 k.y. Much of this record is based on analyses of *Uvigerina*, so that a fairly reliable carbon isotope record also is available. In certain sections, *Cibicides* was analyzed so that the reliability of the $\delta^{13}\text{C}$ record could be evaluated. The $\delta^{18}\text{O}$ record appears to be dominated by variability at the obliquity frequency back to the early Gauss. Below this level, variability is less regular, but there is suffi-

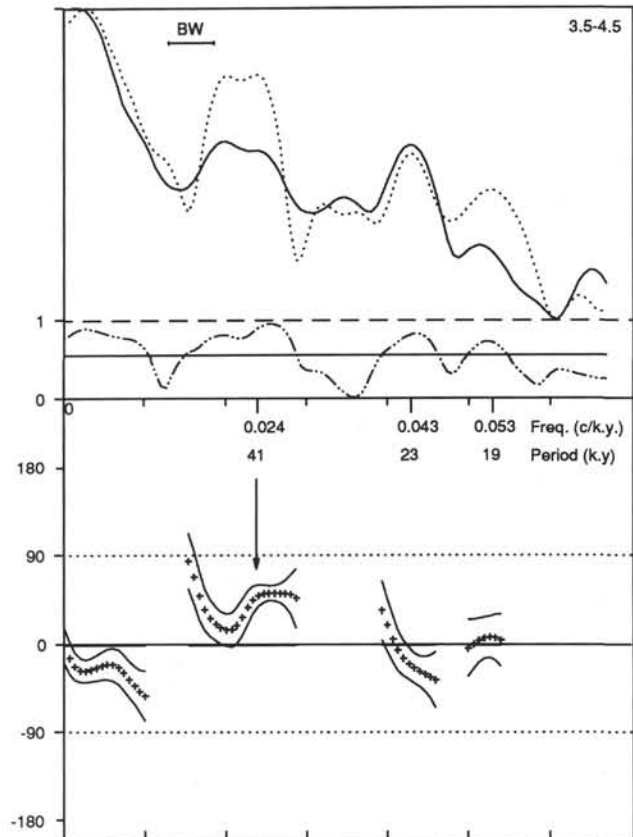


Figure 11. Cross-spectral analysis of $\delta^{18}\text{O}$ (dashed line) vs. GRAPE density (solid line) for Site 846, 3.5 to 4.5 Ma. Coherency is indicated by the lower (dashed/dotted) line. On the phase plot, the main obliquity frequency is marked.

cient variability to justify high-frequency analysis in additional sites. In the lower part of the record, the values are predominantly in the range between modern values and values of about 0.6‰ lighter; this may be explained either by warmer Pacific Ocean Deep Water (by about 2°C), by reductions in Antarctic ice volume (to less than one-half its present volume), or, most likely, a combination of these two factors. Cross-spectral analysis shows during the mid-Pliocene the climate system included a component having a long time constant, strengthening the case for the existence of cyclic fluctuations in the size of the Antarctic ice sheet during that interval.

ACKNOWLEDGMENTS

We are grateful to NERC for support, without which, such a major commitment of stable isotope measurements to a single sequence would have been impossible. We thank Chris Mato, John Miller, and other staff of the Gulf Coast Core Repository at Texas A&M University for enabling us to conduct intensive sampling during our Leg 138 post-cruise meeting, as well as for supplying additional 'fill-in' samples subsequently. We thank Simon Crowhurst for a great deal of help in data handling, and Terri Hagelberg for providing such excellent primary GRAPE density stratigraphy. We are grateful to Maureen Raymo and Ralph Tiedemann for valuable discussion of the extension of the formal oxygen isotope stratigraphy. Discussions and correspondence with Lloyd Burckle, George Denton, Dave Harwood, Dave Hodell, Jim Kennett and Peter Webb, have improved our understanding of the controversy surrounding Pliocene events in Antarctica. We thank Dave Hodell and Eystein Jansen for their careful reviews of the submitted manuscript.

REFERENCES*

- Becker, K., Sakai, H., et al., 1988. *Proc. ODP, Init. Repts.*, 111: College Station, TX (Ocean Drilling Program).
- Berger, A., and Loutre, M.F., 1991. Insolation values for the climate of the last 10 million years. *Quat. Sci. Rev.*, 10:297-317.
- Berggren, W.A., Kent, D.V., and Flynn, J.J., 1985. Jurassic to Paleogene: Part 2. Paleogene geochronology and chronostratigraphy. In Snelling, N.J. (Ed.), *The Chronology of the Geological Record*. Geol. Soc. London Mem., 10:141-195.
- Clapperton, C.M., and Sugden, D.E., 1990. Late Cenozoic glacial history of the Ross Embayment, Antarctica. *Quat. Sci. Rev.*, 9:253-272.
- Coplen, T.B., 1988. Normalization of oxygen and hydrogen isotope data. *Chem. Geol. (Isotope Geosci. Sect.)*, 72:293-297.
- Emiliani, C., 1955. Pleistocene temperatures. *J. Geol.*, 63:538-578.
- Farrell, J.W., 1991. Late Neogene palaeoceanography of the central equatorial Pacific: evidence from carbonate preservation and stable isotopes [Ph.D. thesis]. Brown Univ., Providence, RI.
- Hagelberg, T., Shackleton, N., Pisias, N., and Shipboard Scientific Party, 1992. Development of composite depth sections for Sites 844 through 854. In Mayer, L., Pisias, N., Janecek, T., et al., *Proc. ODP, Init. Repts.*, 138 (Pt. 1): College Station, TX (Ocean Drilling Program), 79-85.
- Hays, J.D., Saito, T., Opdyke, N.D., and Burckle, L.H., 1969. Pliocene-Pleistocene sediments of the equatorial Pacific: their paleomagnetic, biostratigraphic, and climatic record. *Geol. Soc. Am. Bull.*, 80:1481-1513.
- Hilgen, F.J., 1991. Extension of the astronomically calibrated (polarity) time scale to the Miocene-Pliocene boundary. *Earth Planet. Sci. Lett.*, 107:349-368.
- Hodell, D.A., and Venz, K., 1992. Toward a high-resolution stable isotopic record of the Southern Ocean during the Pliocene-Pleistocene (4.8 to 0.8 Ma). In Kennett, J.P., Wamke, D.A. (Eds.), *The Antarctic Paleoenvironment: A Perspective on Global Change* (Pt. 1). *Antarc. Res. Ser.*, 56:265-310.
- Houghton, J.T., Jenkins, G.J., and Ephraums, J.J. (Eds.), 1990. *Climate Change: The IPCC Scientific Assessment*. Cambridge (Cambridge Univ. Press).
- Jenkins, G.M., and Watts, D.G., 1968. *Spectral Analysis and Its Applications*: San Francisco (Holden Day).
- Kastens, K.A., 1992. Did glacio-eustatic sea level drop trigger the Messinian salinity crisis? New evidence from Ocean Drilling Program Site 654 in the Tyrrhenian Sea. *Paleoceanography*, 7:333-356.
- Keigwin, L.D., 1987. North Pacific deep water formation during the latest glaciation. *Nature*, 330:363-364.
- Kennett, J.P., Houtz, R.E., et al., 1974. *Init. Repts. DSDP*, 29: Washington (U.S. Govt. Printing Office).
- Loubere, P., and Moss, K., 1986. Late Pliocene climatic change and the onset of Northern Hemisphere glaciation as recorded in the northeast Atlantic Ocean. *Geol. Soc. Am. Bull.*, 97:818-828.
- Marchant, D.R., Swisher, C.C., III, Lux, D.R., West, D.P., Jr., and Denton, G.H., 1993. Pliocene paleoclimate and East Antarctic ice-sheet history from surficial ash deposits. *Science*, 260:667-670.
- Mayer, L., Pisias, N., Janecek, T., et al., 1992. *Proc. ODP, Init. Repts.*, 138 (Pts. 1 and 2): College Station, TX (Ocean Drilling Program).
- Mix, A.C., Pisias, N.G., Zahn, R., Rugh, W., Lopez, C., and Nelson, K., 1991. Carbon 13 in Pacific deep and intermediate waters, 0-370 Ka: implications for ocean circulation and Pleistocene CO₂. *Paleoceanography*, 6:205-226.
- Raymo, M.E., Hodell, D., and Jansen, E., 1992. Response of deep ocean circulation to initiation of Northern Hemisphere glaciation (3-2 Ma). *Paleoceanography*, 7:645-672.
- Raymo, M.E., Ruddiman, W.F., Backman, J., Clement, B.M., and Martinson, D.G., 1989. Late Pliocene variation in Northern Hemisphere ice sheets and North Atlantic deep water circulation. *Paleoceanography*, 4:413-446.
- Sarnthein, M., and Fenner, J., 1988. Global wind-induced change of deep-sea sediment budgets, new ocean production and CO₂ reservoirs ca. 3.3-2.35 Ma BP. *Philos. Trans. R. Soc. London*, 318:487-504.
- Sarnthein, M., and Tiedemann, R., 1989. Toward a high-resolution stable isotope stratigraphy of the last 3.4 million years: Sites 658 and 659 off northwest Africa. In Ruddiman, W., Sarnthein, M., et al., *Proc. ODP, Sci. Results*, 108: College Station, TX (Ocean Drilling Program), 167-185.
- Shackleton, N.J., 1987. Oxygen isotopes, ice volume, and sea level. *Quat. Sci. Rev.*, 6:183-190.
- Shackleton, N.J., Berger, A., and Peltier, W.R., 1990. An alternative astronomical calibration of the lower Pleistocene timescale based on ODP Site 677. *Trans. R. Soc. Edinburgh, Earth Sci.*, 81:251-261.
- Shackleton, N.J., and Hall, M.A., 1984. Oxygen and carbon isotope stratigraphy of Deep Sea Drilling Project Hole 552A: Plio-Pleistocene glacial history. In Roberts, D.G., Schnitker, D., et al., *Init. Repts. DSDP*, 81: Washington (U.S. Govt. Printing Office), 599-609.
- Shackleton, N.J., and Hall, M.A., 1989. Stable isotope history of the Pleistocene at ODP Site 677. In Becker, K., Sakai, H., et al., *Proc. ODP, Sci. Results*, 111: College Station, TX (Ocean Drilling Program), 295-316.
- Shackleton, N.J., and Imbrie, J., 1990. The $\delta^{18}\text{O}$ spectrum of oceanic deep water over a five-decade band. *Clim. Change*, 16:217-230.
- Shackleton, N.J., and Opdyke, N.D., 1973. Oxygen isotope and paleomagnetic stratigraphy of equatorial Pacific core V28-238: oxygen isotope temperatures and ice volumes on a 10⁵ year and 10⁶ year scale. *Quat. Res. (N.Y.)*, 3:39-55.
- Shackleton, N.J., and Pisias, N.G., 1985. Atmospheric carbon dioxide, orbital forcing, and climate. In Sundquist, E.T., and Broecker, W.S. (Eds.), *The Carbon Cycle and Atmospheric CO₂: Natural Variations Archaean to Present*. Am. Geophys. Union Monogr., 32:303-317.
- Tiedemann, R., 1992. Astronomic tuning of the high-resolution benthic records from ODP Sites 658 and 659 for the last 5 million years vs. non-linear climate dynamics. *GEOMAR Rep.*, 15:282. (Abstract)
- Vincent, E., 1981. Neogene carbonate stratigraphy of Hess Rise (central North Pacific) and paleoceanographic implications. In Thiede, J., Vallier, T.L., et al., *Init. Repts. DSDP*, 62: Washington (U.S. Govt. Printing Office), 571-606.
- Webb, P.N., and Harwood, D.M., 1991. Late Cenozoic glacial history of the Ross Embayment, Antarctica. *Quat. Sci. Rev.*, 10:215-223.

* Abbreviations for names of organizations and publication titles in ODP reference lists follow the style given in *Chemical Abstracts Service Source Index* (published by American Chemical Society).

Date of initial receipt: 17 February 1993

Date of acceptance: 8 October 1993

Ms 138SR-117

Table 7. Interpolated time series of $\delta^{18}\text{O}$ and $\delta^{13}\text{C}$ data for Site 846 as used for time series analysis.

Age (Ma)	$\delta^{18}\text{O}$ (‰)	$\delta^{13}\text{C}$ (‰)	Age (Ma)	$\delta^{18}\text{O}$ (‰)	$\delta^{13}\text{C}$ (‰)
1.763	3.82	-0.35	1.886	3.44	-0.09
1.766	3.78	-0.41	1.889	3.37	0.01
1.769	3.42	-0.18	1.892	3.49	-0.09
1.772	3.51	-0.23	1.895	3.47	-0.07
1.775	-9999.00	-9999.00	1.898	3.52	-0.15
1.778	3.43	-0.13	1.901	3.65	-0.32
1.781	3.76	-0.45	1.904	3.91	-0.38
1.784	3.77	-0.41	1.907	3.92	-0.40
1.787	3.93	-0.52	1.910	4.09	-0.48
1.790	4.09	-0.63	1.913	4.14	-0.40
1.793	-9999.00	-9999.00	1.916	4.27	-0.39
1.796	4.03	-0.64	1.919	3.98	-0.47
1.799	3.94	-0.62	1.922	3.85	-0.36
1.802	4.10	-0.55	1.925	3.90	-0.23
1.805	3.90	-0.42	1.928	3.86	-0.14
1.808	3.89	-0.60	1.931	3.48	-0.13
1.811	3.84	-0.54	1.934	3.50	-0.08
1.814	3.60	-0.34	1.937	3.63	-0.20
1.817	3.59	-0.30	1.940	3.56	-0.25
1.820	3.66	-0.35	1.943	3.61	-0.16
1.823	3.59	-0.44	1.946	3.53	-0.20
1.826	3.64	-0.26	1.949	3.43	-0.37
1.829	3.53	-0.27	1.952	3.68	-0.44
1.832	-9999.00	-9999.00	1.955	3.95	-0.47
1.835	3.65	-0.56	1.958	3.91	-0.47
1.838	3.90	-0.67	1.961	3.79	-0.58
1.841	3.97	-0.54	1.964	3.77	-0.50
1.844	3.65	-0.35	1.967	3.73	-0.44
1.847	3.57	-0.21	1.970	3.58	-0.20
1.850	3.53	-0.23	1.973	3.44	-0.27
1.853	3.38	-0.19	1.976	3.43	-0.07
1.856	3.37	-0.20	1.979	3.32	0.08
1.859	3.53	-0.23	1.982	3.29	-0.32
1.862	3.55	-0.04	1.985	3.73	-0.51
1.865	3.68	-0.12	1.988	3.96	-0.48
1.868	3.80	-0.28	1.991	3.75	-0.36
1.871	3.68	-0.27	1.994	3.75	-0.24
1.874	-9999.00	-9999.00	1.997	3.78	-0.42
1.877	3.61	-0.18	2.000	3.77	-0.41
1.880	3.62	-0.11			
1.883	-9999.00	-9999.00			

Note: For cross spectral analysis the phase between insolation and negative $\delta^{18}\text{O}$ is calculated.

Table 8. Results of cross spectral analysis.

	41k.y.			23 k.y.		19 k.y.	
	Interval	Coh.	Ph.	Coh.	Ph.	Coh.	Ph.
846 GRAPE vs. stack GRAPE	1.8-3	0.82	4±14	0.84	1±13	0.75	-14±17
	3-4	0.87	-7±12	0.85	-3±04	0.83	-25±15
	4-5	0.87	5±12	0.89	3±11	0.71	18±21
	5-6	0.55	-13±31	0.91	7±10	0.76	51±9
846 $\delta^{18}\text{O}$ vs. insolation	1.8-3	0.98	56±04	0.71	-8±19	0.56	-6±27
	3-4	0.85	83±14	0.66	-39±25	0.32	
	4-5	0.87	21±13	0.51	-6±30	0.57	24±29
	5-6	0.32		0.25		0.60	-60±29
846 $\delta^{13}\text{C}$ vs. insolation	1.8-3	0.94	60±07	0.59	42±26	0.24	
	3-4	0.89	58±11	0.38		0.14	
	4.4-5	0.66		0.58		0.28	
	5-6	0.48		0.27		0.74	
846 $\delta^{18}\text{O}$ vs. 846 GRAPE	3.5-4.5	0.93	51±9	0.82	-26±15	0.72	8±21

Note: Coherency (Coh.) is given at the central orbital frequency, and a figure for the phase (Ph.) is only given if the coherency is significant.

Table 9. Data listing for Site 677 with proper ODP identifiers as spliced for time-series analysis (Shackleton, Berger, and Peltier, 1990).

Core, section, interval (cm)	Percentage		δ (m)	Depth (mcd)	Benthic $\delta^{18}\text{O}$	Benthic $\delta^{13}\text{C}$	Planktonic $\delta^{18}\text{O}$	Planktonic $\delta^{13}\text{C}$
	over 150 μm	Depth (mbsf)						
111-677A-								
IH-1, 40	13.2	0.40	0.0	0.40	3.93	-0.05	-2.22	1.54
IH-1, 50	19.3	0.50	0.0	0.50	4.27	-0.20	-1.73	1.37
IH-1, 60	16.9	0.60	0.0	0.60	4.58	-0.28	-1.16	1.42
IH-1, 70	13.2	0.68	0.0	0.68	4.22	-0.32	-1.23	1.30
IH-1, 80	10.4	0.80	0.0	0.80	4.80	-0.50	-1.00	1.61
IH-1, 90	7.3	0.90	0.0	0.90	4.99	-0.39	-0.87	1.15
IH-1, 98	10.7	0.98	0.0	0.98	5.07	-0.41	-0.69	1.05
IH-1, 110	10.1	1.10	0.0	1.10	5.15	-0.29	-0.45	1.55
IH-1, 120	9.8	1.20	0.0	1.20	5.13	-0.37	-0.66	1.09
IH-1, 130	9.5	1.30	0.0	1.30	4.94	-0.34	-0.46	1.17
IH-1, 140	11.8	1.40	0.0	1.40	5.19	-0.21	-0.63	1.06
IH-2, 0	13.5	1.50	0.0	1.50	4.94	-0.23	-0.73	1.22
IH-2, 10	9.8	1.60	0.0	1.60	4.94	-0.24	-0.77	1.39
IH-2, 20	11.0	1.70	0.0	1.70	4.77	-0.32	-0.84	1.48
IH-2, 30	10.3	1.80	0.0	1.80	4.78	-0.21	-0.62	1.79
IH-2, 40	8.7	1.90	0.0	1.90	4.77	-0.20	-0.97	1.48
IH-2, 50	7.5	2.00	0.0	2.00	4.81	-0.21	-1.23	1.32
IH-2, 60	9.6	2.10	0.0	2.10	4.69	-0.19	-1.01	1.19
IH-2, 70	14.3	2.20	0.0	2.20	4.64	-0.22	-1.07	1.28
IH-2, 80	9.8	2.30	0.0	2.30	4.56	-0.28	-1.29	1.40
IH-2, 90	8.8	2.40	0.0	2.40	4.66	-0.20	-1.26	1.33
IH-2, 97	7.9	2.47	0.0	2.47	4.71	-0.12	-1.12	1.37
IH-2, 110	6.4	2.58	0.0	2.58	4.60	-0.25	-1.24	1.00
IH-2, 120	12.9	2.70	0.0	2.70	4.59	-0.17	-1.17	1.34
IH-2, 130	8.9	2.80	0.0	2.80	4.58	-0.38	-1.35	1.17
IH-2, 140	13.6	2.90	0.0	2.90	4.45	-0.39	-1.16	1.41
IH-3, 0	14.8	3.00	0.0	3.00	4.58	-0.14	-1.55	1.23
IH-3, 10	13.5	3.10	0.0	3.10	4.62	-0.18	-1.41	1.22
IH-3, 20	10.7	3.20	0.0	3.20	4.54	-0.33	-1.52	1.20
IH-3, 30	9.8	3.30	0.0	3.30	4.55	-0.43	-1.47	1.19
IH-3, 40	5.9	3.40	0.0	3.40	4.67	-0.37	-1.48	1.84
IH-3, 50	3.8	3.50	0.0	3.50	4.71	-0.33	-1.13	1.33
IH-3, 60	5.6	3.60	0.0	3.60	4.72	-0.39	-1.22	1.40
IH-3, 70	3.9	3.70	0.0	3.70	4.74	-0.35	-1.21	0.94
IH-3, 80	3.3	3.80	0.0	3.80	4.78	-0.36	-1.20	1.17
IH-3, 90	2.4	3.90	0.0	3.90	4.57	-0.14	-1.29	1.43
IH-3, 97	2.5	3.97	0.0	3.97	4.70	-0.32	-1.06	1.54
111-677B-								
IH-3, 40	3.9	3.40	0.7	4.10	4.02	0.03	-1.43	1.51
IH-3, 50	4.4	3.50	0.7	4.20	3.87	NA	-1.59	1.52
IH-3, 60	5.5	3.60	0.7	4.30	3.80	0.14	-1.66	1.68
IH-3, 70	5.5	3.70	0.7	4.40	4.27	0.09	-1.83	1.64
IH-3, 80	4.5	3.80	0.7	4.50	3.74	0.20	-1.91	1.65
IH-3, 90	4.9	3.90	0.7	4.60	3.72	0.06	-1.79	1.59
IH-3, 98	4.9	3.98	0.7	4.68	4.07	-0.03	-1.58	1.47
IH-3, 110	3.9	4.10	0.7	4.80	4.08	-0.06	-1.18	1.74
IH-3, 120	3.7	4.20	0.7	4.90	4.16	0.01	-1.66	1.67
IH-3, 130	4.2	4.30	0.7	5.00	3.99	-0.01	-1.74	1.85
IH-3, 140	6.8	4.40	0.7	5.10	3.83	-0.08	-1.71	1.74
IH-4, 10	4.3	4.60	0.7	5.30	3.85	-0.17	-1.91	1.68
IH-4, 20	6.1	4.70	0.7	5.40	3.99	-0.24	-1.85	1.55
IH-4, 30	3.4	4.80	0.7	5.50	4.14	-0.23	-1.73	1.47
IH-4, 40	3.1	4.90	0.7	5.60	3.48	-0.27	-1.44	1.71
IH-4, 50	5.5	5.00	0.7	5.70	3.72	-0.22	-1.81	1.38
IH-4, 60	4.1	5.10	0.7	5.80	3.88	NA	-1.83	1.52
IH-4, 70	3.4	5.20	0.7	5.90	3.95	-0.11	-1.73	1.68
IH-4, 80	7.3	5.30	0.7	6.00	3.65	-0.17	-2.50	1.35
IH-4, 90	1.9	5.40	0.7	6.10	3.83	-0.08	-1.70	1.18
IH-4, 98	5.1	5.48	0.7	6.18	4.28	-0.21	-1.34	0.75
IH-4, 110	7.1	5.60	0.7	6.30	4.88	-0.31	-0.51	0.89
IH-4, 120	9.8	5.70	0.7	6.40	4.76	-0.27	-0.53	0.86
IH-4, 130	8.7	5.80	0.7	6.50	5.02	-0.37	-0.57	0.91
IH-4, 140	7.2	5.90	0.7	6.60	5.10	-0.42	-0.57	0.88
IH-5, 0	6.6	6.00	0.7	6.70	5.08	-0.50	-0.56	1.09
IH-5, 10	5.8	6.10	0.7	6.80	4.76	-0.81	-0.65	0.88
IH-5, 20	5.3	6.20	0.7	6.90	4.95	NA	-0.78	0.89
IH-5, 30	5.6	6.30	0.7	7.00	4.89	NA	-0.95	0.81
IH-5, 40	4.6	6.40	0.7	7.10	4.89	NA	-0.95	1.04
IH-5, 50	3.5	6.50	0.7	7.20	4.87	-0.50	-0.57	0.96
IH-5, 60	3.6	6.60	0.7	7.30	4.95	-0.53	-0.87	0.61
IH-5, 70	3.6	6.70	0.7	7.40	4.78	-0.66	-0.60	1.20
IH-5, 80	3.2	6.80	0.7	7.50	4.66	NA	-0.71	0.85
IH-5, 90	3.5	6.90	0.7	7.60	4.92	-0.46	-0.60	1.12
IH-5, 98	3.5	6.98	0.7	7.68	4.82	-0.61	-0.69	0.94
IH-5, 110	2.9	7.10	0.7	7.80	4.72	-0.60	-0.79	1.05
IH-5, 120	4.1	7.20	0.7	7.90	4.69	-0.55	-0.75	0.73
IH-5, 130	2.8	7.30	0.7	8.00	4.60	-0.46	-1.14	0.94

Note: The figure delta (m) is added to the depth mbsf to generate a depth mcd (meters composite depth) as was done for the Leg 138 data (Hagelberg et al., this volume). The benthic $\delta^{18}\text{O}$ and $\delta^{13}\text{C}$ data shown are averages of all analyses in the sample, adjusted for species-dependent departures from isotopic equilibrium. Balance of table on CD-ROM.